In-situ Compact Time-Domain Nuclear Magnetic Resonance for Real-Time Water Quality Monitoring

by

Daniel Hancock

Bachelor of Science
Bridgewater College 2022

Submitted in Partial Fulfillment of the Requirements

for the Degree of Master of Science in

Physics

College of Arts and Science

University of South Carolina

2025

Accepted by:

Thomas Crawford, Director of Thesis

Austin R.J. Downey, Reader

Ann Vail, Dean of the Graduate School

Abstract

Time-domain Nuclear Magnetic Resonance (TD-NMR) is a technique that probes nuclear spin for a variety of purposes, including studying material composition. Measuring at confined frequencies and focusing on relaxation time rather than chemical shift allow TD-NMR systems to be much smaller and more portable than traditional NMR systems. This work reports on the development of a compact TD-NMR system designed for in situ 1H measurements as well as a study using in-situ NMR data and water quality data to predict the concentration of Cu(II) aqueous ions in Rocky Branch Creek. Previous studies have shown that TD-NMR is capable of describing a linear relationship between paramagnetic contaminant concentration and relaxation rate. However, this linear relationship is dependent upon several factors such as the temperature of the electronics and the frequency of the measurement. When measuring in situ, these differences can be significant; knowing the relaxation rate does not indicate knowing Cu(II) ion concentration. To account for this, a machine learning model utilizing random forests is implemented using training data from NMR measurements with different concentrations of paramagnetic Cu(II) aqueous ions in combination with water quality data and time domain signal metrics in order to estimate Cu(II) concentration. This model achieved an R^2 of 0.999 and a mean squared error of 12 mg/L. In the future, this work can be expanded by further compacting the NMR system to enhance portability, by incorporating the machine learning model with the data acquisition system to provide real time predictions, and by enhancing the machine learning model with the capability to distinguish contaminants.

Table of Contents

List of Tables

List of Figures

Chapter 1

Introduction

Nuclear Magnetic Resonance (NMR), broadly speaking, is a technique revolving using magnetic fields to probe the magnetic behavior of atomic nuclei. It is a valuable tool across chemistry, biology and material science due to its ability to provide insight into chemical environments and molecular interactions. Traditional high-field NMR systems offer exceptional resolution, but are costly, bulky, and require specialized infrastructure, often limiting them to laboratory settings. One example of this is Magnetic Resonance Imaging (MRI), which is based on the principles of NMR and uses the relaxation properties of nuclei to generate detailed images of soft tissue. Ordinarily, these MRI systems are large bulky, and immovable, however, recent advancements in portable, low-field MRI, such as point-of-care systems utilizing ultralow-field permanent magnets [3], have dramatically reduced these requirements. These developments increase accessibility in medical imaging while increased component availability also enables the creation of compact, low-cost NMR systems for field applications like environmental monitoring and fuel analysis.

With this development, Compact NMR has become an established field [5], driven by advances in magnet design [8] that allow permanent magnets to achieve the homogeneity needed for applications previously restricted to high-field systems [2]. While high-field NMR remains indispensable for tasks requiring extremely high resolution, compact low-field NMR systems now offer a practical, cost-effective alternative for routine analysis and field applications. These systems, often referred to as desktop or mobile NMR [6], enable multi-nuclear and multi-dimensional NMR relaxometry

or spectroscopy on the benchtop, making them accessible for chemical analysis, reaction monitoring, and nondestructive evaluation. With applications ranging from food industry quality control [16] to the monitoring of oil wells [40], compact NMR [33] instruments have proven valuable in diverse settings. Their portability and ease of use have opened up new possibilities for real-time, on-site analysis in fields like environmental monitoring [30] and process control [25], without the need for the expensive infrastructure or maintenance associated with high-field NMR.

Various open-source NMR systems have emerged, each tailored to specific applications. For example, the NMRduino platform by Tayler and Bodenstedt emphasizes accessibility for educational purposes and simplicity in hardware setup, making it ideal for users seeking to understand basic NMR principles at low cost [39]. However, its limited frequency range restricts its ability to resolve fine chemical shifts, making it less suited for advanced applications requiring higher sensitivity. Similarly, Louis-Joseph and Lesot's FT-NMR system is a low-cost benchtop spectrometer optimized for teaching and basic molecular analysis [26]. While cost-effective, this system's benchtop focus limits its applicability to field studies. In contrast, Bryden et al. developed an ultra-low-field (ULF) NMR system featuring RF mixing and pre-polarization, enhancing signal strength and resolution, making it well-suited for hyperpolarized gas detection [9]. However, its low field strength may limit sensitivity for applications requiring high spectral resolution. These systems provide a foundation to build upon, paving the way for more systems to be developed. To understand how a new NMR system can be developed, a solid theoretical framework for how NMR can work with smaller magnets must first be discussed.

Since NMR is a property relating to nuclear spin, understanding NMR requires an understanding of nuclear spin, its corresponding energy, and its behavior in an external magnetic field. Nuclear spin is denoted by I and can be represented with the nuclear spin quantum number, m. The multiplicity of spin states is equal to $2I+1$

and is associated with quantum numbers in the value of $m = -I, -I+1, ..., I-1, I$. When placed in an external magnetic field, these states have different energies, given by:

$$E_i = -m_i \frac{\gamma h B_0}{2\pi}, \tag{1.1}$$

where E_i is the energy of a nuclear spin state, i, m_i is the nuclear spin quantum number of this spin state, γ is the gyromagnetic constant characteristic of the specific isotope in the field, h is Planck's constant, and B_0 is the magnetic field strength [28]. The significance of this effect in regards to NMR comes into play when discussing distribution. Before a group of particles in thermal equilibrium is placed in a magnetic field, all of the nuclear states are degenerate, meaning that the probability of any particle being in any energy state is the same for all particles and all possible energy states. After being placed in the field, it is intuitive to think that there would be an equal number of particles aligned and antialigned with the magnetic field based on the spin state that particle is in. This can be problematic when probing magnetic properties because it implies that the overall magnetization of a sample is 0 [28, 18]. If this is the case, how would it be possible to study the magnetization? As Equation 1.1 shows, in an external magnetic field, particles with nuclear spin aligned with the field have a lower energy than particles with nuclear spin anti-aligned with the field. When different energy states are available, quantum mechanics via the Boltzmann Distribution describes how lower energy states are preferred, as given by:

$$\frac{P_{m=-1/2}}{P_{m=1/2}} = e^{-\Delta E/kT}, \tag{1.2}$$

where P represents the fraction of particles in each spin state, ΔE is the change of energy between the two spin states that can be calculated using Equation 1.1, k is the Boltzmann constant, and T is the temperature in Kelvin [28]. Because of this, when a collection of particles is placed in a magnetic field, there will be more particles with nuclear spins aligned with the magnetic field, creating a net magnetization in the

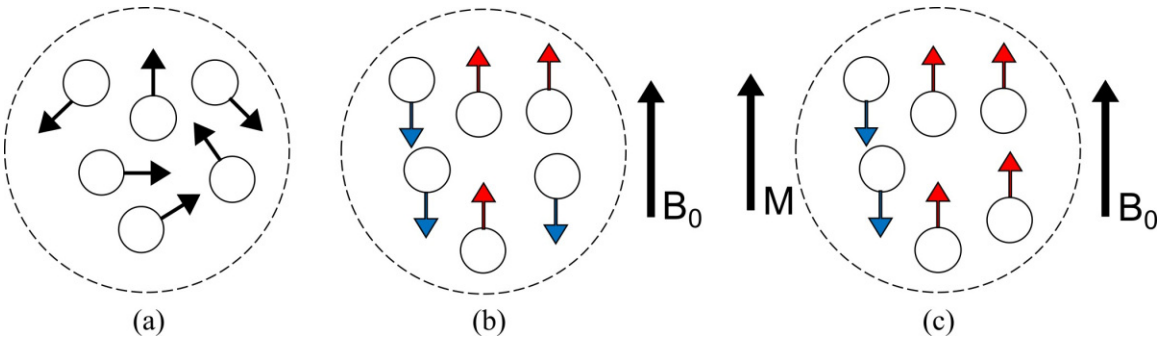

Figure 1.1: Populations of particles showing: (a) the degenerate case, (b) a population placed in a magnetic field, and (c) a population placed in a magnetic field considering the Boltzmann Distribution.

same direction as the external field, making NMR possible [28, 18, 19, 11]. Figure 1.1 shows an example of these different states, from the initial degenerate case to the current case resulting in a net magnetization.

Those familiar with quantum mechanics will know that there is another substantive problem with this picture. If the spin lies perfectly in the z-direction, then the spin in the x and y-directions must be 0. In this case, all three spins are known, violating quantum uncertainty. Because of this, the spin and magnetic moment of the particle will try to align with the external magnetic field, but will be bounded off-axis by quantum uncertainty. There is still a net magnetization in the direction of the applied field due to the preference of lower energy states, but in general, the direction of the spin for an individual particle is still mostly random . Furthermore, since the spin and magnetic moment are not perfectly aligned with the external magnetic field, a torque will be induced, causing changes in angular momentum and initiating precession of the magnetic moment around the external field [28, 18, 19, 11].

While using quantum mechanics can describe how the particle behaves, it is much more simple to derive the numerical behavior of the particle with classical mechanics. A particle's magnetic moment, μ can be decribed as:

$$\mu = \frac{1}{2}\int r \times J(r) d^3r = \frac{1}{2}\int r \times \sigma(r) v(r) d^3r, \tag{1.3}$$

where r is the radial coordinate, $J(r)$ is the current density, $\sigma(r)$ is the electric charge

density, and $v(r)$ is the drift velocity of the particle. This is quite similar to the equation for angular momentum, L, given by,

$$L = \int r \times \rho(r) v(r) d^3 r, \tag{1.4}$$

where ρ is the mass density. Substituting L in Equation 1.4 results in a simple relation for particles that have proportional mass and electric charge densities:

$$\mu = \gamma L. \tag{1.5}$$

Utilizing the relation between torque, τ, and angular momentum ($\frac{dL}{dt} = \tau$), as well as the definition of magnetic torque ($\tau = \mu \times B$), the angular frequency describing the precession of the particle is:

$$\omega_0 = \gamma B, \tag{1.6}$$

where ω_0 is known as the Larmor frequency. This is a significant result, showing that the precession of a particle's magnetic moment around an external field is determined by a physical constant of the specific isotope and the strength of the external magnetic field. With this, changing the external magnetic field for known particles allows for the precession frequency to be controlled [19]. Figure 1.2 shows two examples of what this precession can look like.

By placing particles in an external magnetic field, a net magnetization and Larmor precession have been introduced to the system. An interesting extension to this idea is thinking about what happens if another external magnetic field is added. If a static magnetic field is added, due to superposition, it would be like there is only one field, just in a direction that is a linear combination of the two static fields. In order to create an effect on sample nuclei, the secondary magnetic field must oscillate. However, since the nuclear spins are precessing, an oscillating magnetic field at some random frequency will sometimes push and sometimes pull on those nuclei, not resulting in any significant change. However, if the secondary magnetic field is oscillating

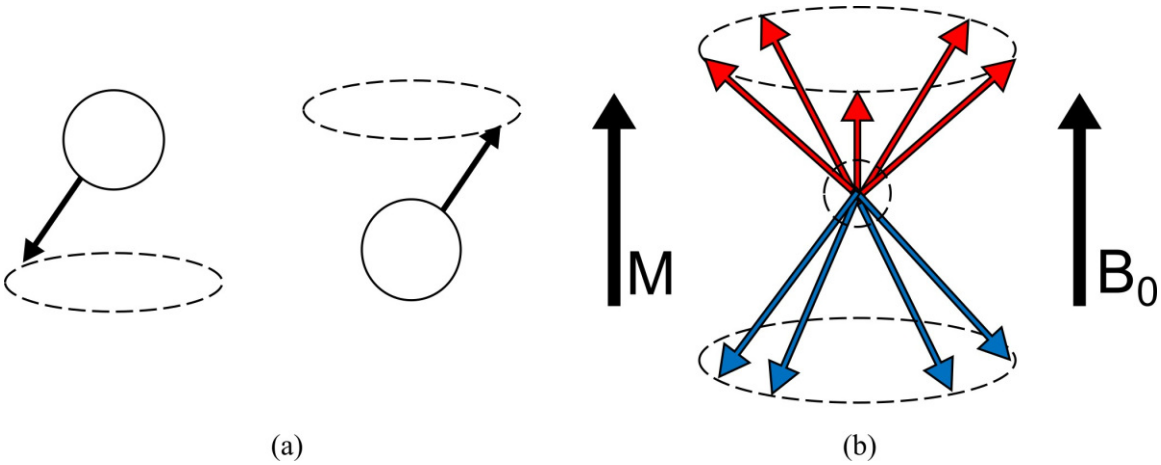

Figure 1.2: Larmor precession examples showing: (a) two individual nuclei precessing, (b) a population of nuclei precessing in an external field with a net magnetization due to the Boltzmann Distribution.

at the same frequency as those nuclei, the effect will remain constant, allowing for manipulation of the overall magnetization of the sample. Due to geometry, this effect is maximized when the secondary oscillating magnetic field is perpendicular to the original static magnetic field. With this, if the original field is in the z-direction and the secondary oscillating field is in the y-direction, the magnetization of the sample will rotate around the y-axis. It is important to note that the precessing behavior will resume, so while the magnetization is rotating around the y-axis, it will be precessing around the z-axis. It is also important to remember that this magnetization is caused by the overall preference of the nuclei in the sample to follow the oscillating magnetic field [28, 18, 19, 11]. Because of this, if something causes some of the nuclei to precess faster or slower than that oscillating field, then the net magnetization will decrease over time. This is very important when it comes to NMR relaxation. Figure 1.3 shows how this situation unfolds.

An interesting question in regards to NMR is what happens if the particles are then removed from the magnetic field? Do the magnetization and precession immediately revert back to their previous behavior, do they oscillate to their previous behavior, or do they decay to their previous behavior. The field of NMR relaxometry probes

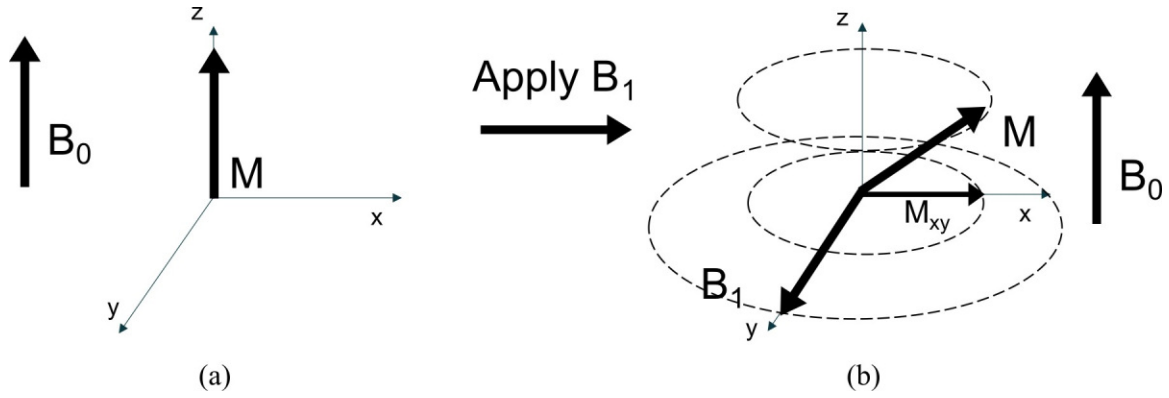

Figure 1.3: Figures showing (a) the magnetization of a population of particles in an external magnetic field and (b) the changes that occur when an oscillating magnetic field in the y-direction is applied.

precisely this.

Before describing NMR relaxometry, it is useful to discuss the convention of the rotating reference frame. It can be exhaustive to think about systems with multiple spins aligned and antialigned while precessing around the external field, particularly when another external magnetic field is introduced, causing the net magnetization to shift out of alignment with the initial field. Because of this, the rotating frame is designed so that the observer, the x-axis, and the y-axis are all rotating around the z-axis at the Larmor frequency, with new coordinate axes, x', y', and z'. This simplifies visualizing NMR greatly because now, any magnetization off of the z-axis, any additional oscillating magnetic field, and any other properties precessing with the Larmor frequency can now be visualized with simple vectors rather than complex rotational diagrams. This will become especially important when discussing T_2 relaxation. Furthermore, in regards to the mathematics of these oscillations, in the lab frame, many of the quantities involved are time dependent [28]. The rotating reference frame can be used to remove this time dependence. Figure 1.4 shows how Figure 1.3 changes when viewed in the rotating reference frame.

There are two types of relaxation that are important to understand regarding NMR. Spin-lattice relaxation describes the process of the net magnetization being

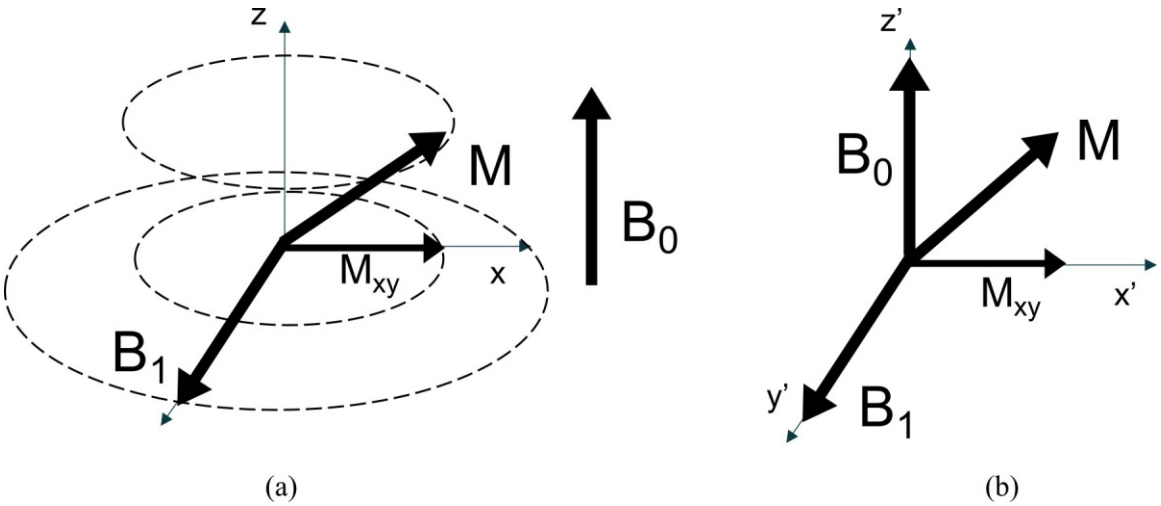

Figure 1.4: Oscillating magnetic field precession in the (a) lab reference frame and (b) the rotating reference frame.

gained from the collection of particles being placed in an external magnetic field to decay after being removed from the field. This relaxation is characterized by the T_1 decay constant [28].

Spin-spin relaxation is a more complicated topic. As discussed previously, if a secondary magnetic field perpendicular to the original external field is pulsed at the Larmor frequency on the y-axis, the net magnetization will begin to rotate in the z-x plane, resulting in a magnetization component in the x-y plane. Spin-spin relaxation describes the decay of the component of the net magnetization in the x-y plane and is characterized by the T_2 decay constant [15]. There are several things that contribute to this decay [14]. As discussed previously, if there is a process that causes some nuclei to precess faster or slower than the oscillating field, the component of magnetization in the x-y plane will decrease. The most prominent factor affecting this is the dipole-dipole interaction. Essentially, if the spin of one nucleus is nearly aligned with the static magnetic field in the z-direction, then a nearby nucleus will not only feel the static magnetic field, but also the magnetic moment of the other nucleus. This increases the larmor frequency and indicates that this nucleus no longer precesses with the net magnetization, contributing to the relaxation of the sample [12].

One important thing to note is that the strength of this interaction is proportional to the gyromagnetic ratio. Because of this, paramagnetic material in the sample will contribute very strongly to relaxation due to the higher gyromagnetic ratio of the unpaired electrons [13].

Measuring relaxation is also not a very straightforward process. An NMR relaxometry signal contains magnetic oscillations due to the precession of the net magnetization in the sample. The most simple way to acquire this signal is by using the oscillating magnetization to induce a current in some kind of wire, specifically a coil due to favorable geometry. If the coil is in the x-y plane, it will be able to receive an induced current any time there is an oscillating magnetization in the x-y plane. Furthermore, as mentioned previously, if a magnetic field oscillating with the Larmor frequency is applied perpendicular to an external magnetic field, the net magnetization begins to rotate into the around the y-axis, resulting in a component in the x-y plane [28]. Because of this, not only can the coil be used to collect signal, but also to generate the NMR signal itself.

With this in mind, spin-lattice relaxation can be observed through a process called inversion-recovery. In this process, an oscillating magnetic field is applied for a time long enough for the magnetization to anti-align with the external field. After this pulse is applied, the magnetization will start to shift to its initial direction before the pulse was applied. Any time after that, another oscillating magnetic field is applied to rotate the magnetization into the x-y plane. From there, an induced current can be seen that decays as the magnetization decays. Probing small intervals of different times between the two pulses will eventually result in a measurement that has no induced current, showing a full decay and providing the T_1 decay time. The decay equation for this technique is:

$$M(t) = M(0)(1 - 2\exp(t/T_1)), \tag{1.7}$$

where $M(t)$ is the magnetization at time t, and $M(0)$ is the magnitude of the mag-

netization immediately before the first pulse is applied. The factor of 2 in front of the exponential comes from the nature of this technique, where the magnetization is initially $-M_0$ and it decays to M_0, resulting in $2M(0)$ difference [28]. Since this measurement process revolves around finding when the magnetization in the x-y plane is 0, magnet inhomogeneities can artificially diminish the signal earlier than relaxation, making this technique difficult with magnet inhomogeneities.

Spin-spin relaxation can be observed by the Spin Echo Technique. If an oscillating magnetic field is applied for a short time, resulting in a 90 degree rotation of the magnetization (this is referred to as a 90 degree pulse) is applied to the sample, the magnetization lies in the x' direction. If the magnet is not perfectly homogeneous, the particles will precess slightly differently over a time, τ. This is because the slight difference in magnetic field strength felt by different nuclei result in slight differences to the Larmor frequencies of different nuclei. From this point, if a 180 degree pulse is applied, the slightly spread out magnetization will now be in the -y' direction. Each individual particle will continue precessing the same way it was before the pulse was applied, but due to the geometry of the rotation due to the pulse, they precess back to alignment at $t = \tau$. This process of nuclear magnetic moments realigning is called a spin echo. More 180 degree pulses are applied, waiting τ seconds between each pulse, creating a series of spin echoes. By recording each spin echo until the sample is fully relaxed, spin-spin relaxation can be observed and the T_2 relaxation time can be measured. The equation representing this decay is:

$$M_{xy}(t) = M_{xy}(0)e^{-t/T_2}, \tag{1.8}$$

where $M_{xy}(t)$ is the magnetization in the x-y plane at time t and $M_{xy}(0)$ is the initial magnetization immediately after the first pulse is applied. An important thing to note is that since the pulse pattern described here cancels out the effect of magnet inhomogeneities, this is a versatile technique able to be leveraged by less-ideal magnets

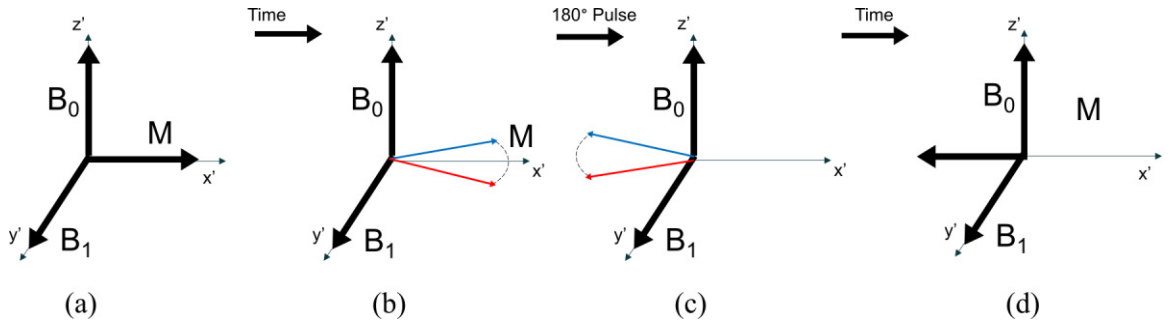

Figure 1.5: Figure showing the T2 relaxation process where (a) is the sample immediately after a 90 degree pulse is applied, (b) is the sample after some time τ after the pulse, (c) is the sample after a 180 degree pulse is applied, and (d) is the sample some time τ after the 180 degree pulse.

[28, 18, 11]. A visualization of this process in the rotating reference frame can be seen in Figure 1.5.

The significance that spin-spin relaxation is unharmed by inhomogeneities in the magnet cannot be understated. This single-handedly allows spin-spin relaxation to be measured through small, portable magnets that are capable of field deployment, serving as the foundation for this thesis.

The contributions of this work are threefold: (1) an open source time-domain NMR system has been developed, implemented, and tested; (2) that system has been adapted and temperature controlled for continuous field deployment and analysis; and (3) extensive amounts of experimental testing have been done to develop and test a machine learning model to predict the magnetic content of water during this field deployment.

Chapter 2

Open-Source Compact Time-Domain Hydrogen (1H) NMR System for Field Deployment

[1] This chapter presents a compact, low-cost TD-NMR system based on a 0.5 T permanent magnet designed for in-situ ^{1}H measurements as well as serving as a tutorial for reproducability of the system. The hardware employs an off-the-shelf data acquisition and control system along with a custom PCB for signal conditioning, ensuring straightforward deployment and reduced costs. The system's core sequence is a Carr-Purcell-Meiboom-Gill pulse train, chosen for efficient T_2 relaxation measurements under varying magnetic susceptibilities. By focusing on relaxation measurements, this approach bypasses complexities of high-resolution spectroscopy, enhances signal-to-noise in low-field conditions, and enables robust characterization across challenging environmental settings. We validate the system using aqueous Copper(II) sulfate solutions, correlating T_2 values with copper concentrations to simulate environmental heavy metal contamination monitoring. Prior work has demonstrated versatility in fuel property analysis and environmental sensing, confirming broad applicability for this portable platform. While packaging and integration with ancillary equipment (e.g., flow-through systems) are not covered, the platform serves as a versatile foundation for specialized deployments. Its open-source design and affordability aim to democratize NMR technology and extending its utility beyond conventional labora-

[1] Winford Janvrin, Jacob Martin, Daniel Hancock, Austin Downey, Perry Pellechia, Joud Satme, and Sang Hee Won, Open-source campact time-domain Hydrogen (1H) NMR system for field deployment, (2025). HardwareX, Elsevier Publications. Reprinted here with permission of the publisher, 2025

tory environments. This accessible configuration fosters widespread educational and professional use [24].

2.1 Hardware in context

Our compact open-source time-domain NMR (TD-NMR) system [4] (shown in Figure 2.1) addresses the limitations of traditional high-field Nuclear Magnetic Resonance (NMR) by offering a versatile, low-cost, and portable solution specifically for hydrogen (^{1}H) NMR applications. Unlike traditional NMR systems, which often require liquid helium-cooled superconducting magnets and extensive infrastructure, our TD-NMR utilizes permanent magnets and simplified electronics, enabling easy operation in field environments. This portability and affordability make it well-suited for applications such as fuel quality analysis [29, 21], environmental monitoring [30, 20], and other in-situ assessments such as online process control or material characterization. By focusing on hydrogen NMR, our system maximizes sensitivity and accessibility, providing a practical alternative to high-field systems for diverse scientific and applied research needs outside of conventional lab settings.

Our compact time-domain NMR system builds on previous open source systems by extending functionality with a focus on versatility and field deployment. Designed for robustness in demanding environments, it supports higher operational frequencies and automatic tuning, enabling use by non-expert users for in-situ applications like environmental monitoring and fuel analysis. While previous systems cater to specific educational or niche scientific needs, our system's modular open-source design allows for extensive customization, making it suitable for a wide range of research applications requiring reliable NMR measurements beyond the lab.

In previous studies, the TD-NMR system developed in this work (Figure 2.1) has proven its adaptability and utility across multiple contexts. Initially, it was employed to measure hydrogen content in gas turbine fuels, where it provided rapid and accu-

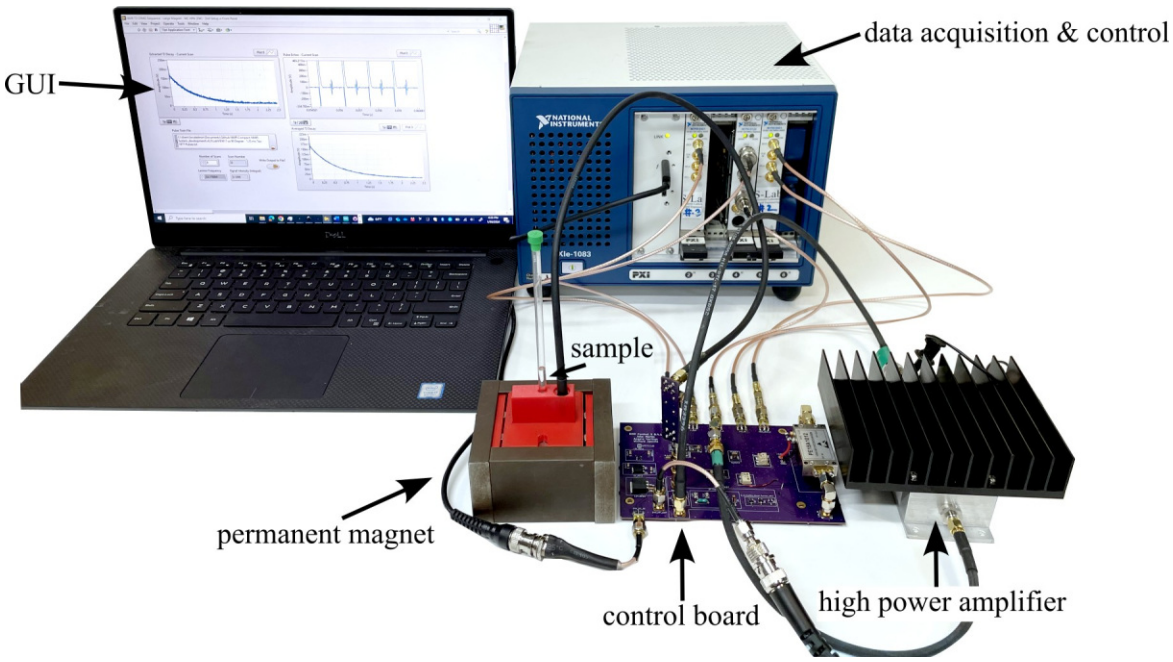

Figure 2.1: Full setup for the compact TD-NMR system, with key components and subsystems annotated.

rate determinations of hydrogen mass percentages, crucial for evaluating combustion properties [29]. The system has also been utilized to assess cetane numbers in jet fuels. By analyzing T_2 relaxation curves, the system predicts the derived cetane number with high accuracy, enabling real-time fuel quality assessments that traditional ASTM standards would typically handle in a more time-consuming manner [21] Subsequently, the system was adapted to track magnetic particle concentrations in wildfire ashes and runoff [30] and quantifying algae uptake of heavy metals [20] highlighting its effectiveness in environmental monitoring scenarios.

The adaptability of this compact TD-NMR system across diverse applications underscores its potential as a valuable tool for both research and practical deployment. Its open-source nature allows users to tailor the system to specific needs, making it a cost-effective and scalable solution across various scientific disciplines. The contributions of this hardware are:

1. The first open-source, low-cost NMR system that combines portability, permanent magnets, and customizable electronics, specifically designed for field-

deployable, in-situ measurements. Unlike previous designs, this system uniquely enables real-time monitoring outside of traditional laboratory environments.

2. A well-developed and extensively validated system, having demonstrated its efficacy in multiple peer-reviewed scientific publications across a range of applications. This includes studies on fuel characterization, magnetic particle quantification in environmental samples, and algae analysis.

2.2 Hardware description

This section describes the hardware, software, and sufficient theory required for the reader to understand the developed open-source compact TD-NMR system.

Overview

The NMR system was developed with the following design goals:

1. Small system that could be further developed into a deployable system
2. Simplistic design with no shim coils that could be easily replicated
3. Achieve clear time domain T_2 NMR results

The NMR system was developed with a foundation based on a custom printed circuit board (PCB) for all the analog signal processing and an off-the-shelf data acquisition and control system built around PXI cards from National Instruments and controlled through a custom LabVIEW code, as shown in Figure 2.1. The use of an off-the-shelf data acquisition was done to minimize the challenges and intricacies involved in developing a precise signal generation and data acquisition system. If properly designed, a custom data acquisition and control system could replace the PXI-based system, greatly reducing overall cost. The compact-NMR uses the NI PXIe-1083 chassis with three modules. These include two NI PXI-5421 cards for signal generation and an NI PXI-5124 card for triggering and collecting the signals. Data is transferred back to the host computer using a Thunderbolt connection. While

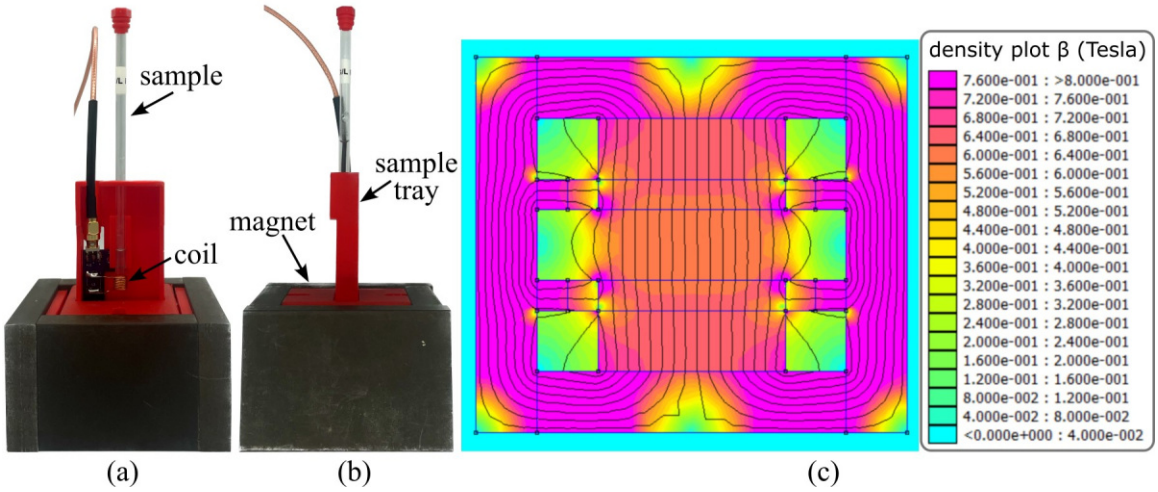

Figure 2.2: Magnet overview, showing: (a) Front view of assembled magnet configuration with tray and coil; (b) side view of assembled magnet configuration and (c) two-dimensional finite element simulation [31].

contemporary off-the-shelf NMR solutions offer exceptional precision in measurements and are meticulously calibrated to enable high-resolution assessments, they are typically configured to operate at fixed frequencies without the flexibility of adjustment. The system presented in this work allows for precise data to be collected and with simple adjustments in the LabVIEW code, it is possible to change frequency, timing, and manipulation of the signal generation. This enables users to modify the system, according to their own specific needs.

Magnet Design

Magnet design for compact NMR is a constantly progressing field that has developed a large number of magnets suitable for use in compact NMR systems. For example, Moresi and Magin developed a miniature permanent magnet for NMR applications capable of achieving a high homogeneity (10 ppm over a $3 \times 3 \times 5$ mm^3 volume) at 0.6 T, scalable up to 3 T through additional magnetic layers, suitable for portable field-deployable NMR systems [32]. Polishchuk and Gardeniers introduced a compact permanent magnet for NMR relaxometry with a novel integration of soft-magnetic

stainless-steel plates in the airgap, significantly enhancing field homogeneity for microfluidic flow measurements [35]. Raich and Blümler developed a dipolar Halbach array utilizing identical bar magnets to create a homogeneous magnetic field, optimizing the array for mobile NMR devices by balancing field strength, homogeneity, and weight [36]. Alnajjar et al. utilized 3D printing with a stainless steel-PLA composite, to develop lightweight, high-performance NMR magnets for portable applications [2].

In Chapter 1, it was described how T2 relaxation was unaffected by inhomogeneities of the magnet. While that is true, there is a tradeoff between signal strength and inhomogeneities. So while the magnet does not have to be homogeneous to industry standards, it is worth trying to optimize homogeneity given the constraint of portability in order to maximize signal strength. The more uniform the magnetic field, the higher the quality of the NMR signal, enhancing signal clarity and accuracy [8]. However, this uniformity narrows the bandwidth of frequencies that effectively excite the sample, necessitating a more precisely calibrated excitation signal. Additionally, environmental temperature changes can impact the magnet's strength, a significant consideration for compact NMR systems used in field applications. These variations can make tracking the excitation bandwidth challenging in magnets with highly homogeneous fields. In brief, high homogeneity results in better signal strength but comes at the cost of overall signal robustness, and this trade-off in magnet design is a variable that should be considered by system developers.

The design presented in this work is a center-field magnet with a steel housing and steel pole shoes [7]. This design was chosen as it it relatively low-cost, easy to reproduce, the the steel housing constrains the magnetic field making the magnet assembly easier to handle once assembled. The magnet assembly features two main N42 neodymium-iron-boron (NdFeB) magnets with dimensions of $3.81 \times 3.81 \times 1.27$ cm as well as eight aligning magnets made of the same material with dimensions of $3.81 \times 0.635 \times 0.635$ cm. These aligning magnets make the magnet stronger and

greatly increase homogeneity. 1018 steel is used to provide a return path for the magnetic flux, making the magnet stronger and significantly safer to handle [30]. The developed permanent magnet is shown in Figure 2.2 and has a Larmor frequency of 24 MHz ±2% while maintaining a small footprint of 90 × 80 × 50 mm with a protective metal casing. When assembled, but without the tray or coil, the magnet weighs 1.99 kg. Figure 2.2(a) and Figure 2.2(b) depict the fully assembled magnet. Figure 2.2(c) shows a 2D Finite Element Method Magnetics (FEMM) [31] simulation of the magnet design. It shows how the 1018 steel bars provide a pathway for magnetic flux as well as depicting the field strength of the magnet. The field strength in the center of the magnet can differ by approximately ±0.2 T according to the simulation, providing an estimation of field inhomogeneity.

Pulse Sequence

The method of applying a 90 degree pulse followed by a series of 180 degree pulses introduced in Chapter 1 when discussing the Spin Echo Technique is specifically referred to as the Carr-Purcell-Meiboom-Gill (CPMG) technique [10], which can be visualized in Figure 2.3. To make this happen with the hardware used in this NMR system, a square wave is generated along with a sine wave. The square wave is used to control when the sine wave is allowed to pass through the coil. The sine wave is used to create the NMR response in the sample. With this technique, as described in Chapter 1, a T2 curve is generated by taking the peak of the NMR signal between pulses, the spin echo. Figure 2.4 depicts what CPMG sequence looks like in regards to the pulses and the spin echoes. In this method, the NMR system can produce clear resolution time domain results while maintaining a small compact footprint that, unlike other NMR systems, does not require any shim coils [22] or complicated calibration to achieve.

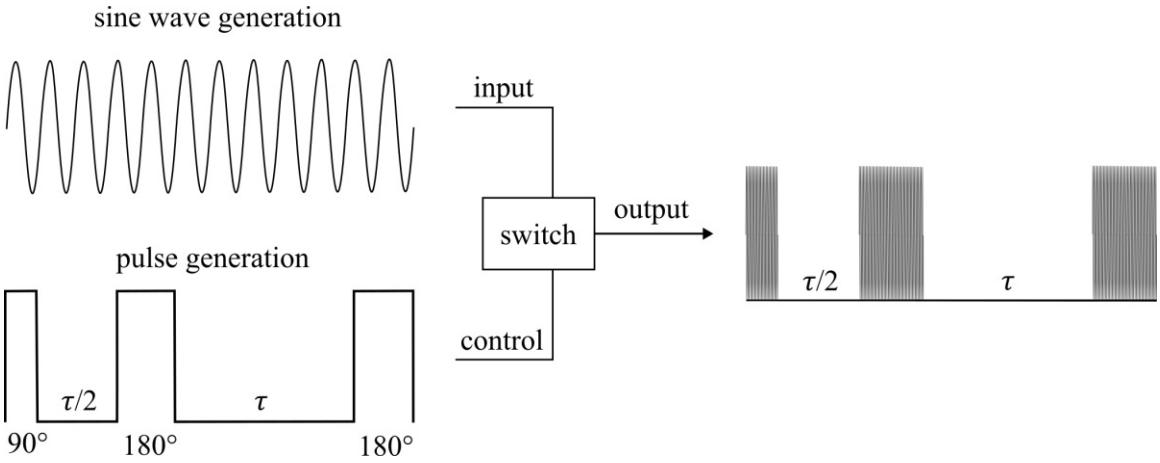

Figure 2.3: The CPMG technique where a square pulse wave acts as the control for the switch, while the sin wave acts as the input. When the square wave is high it activates the switch letting the sin wave travel through creating a pulsed sine wave.

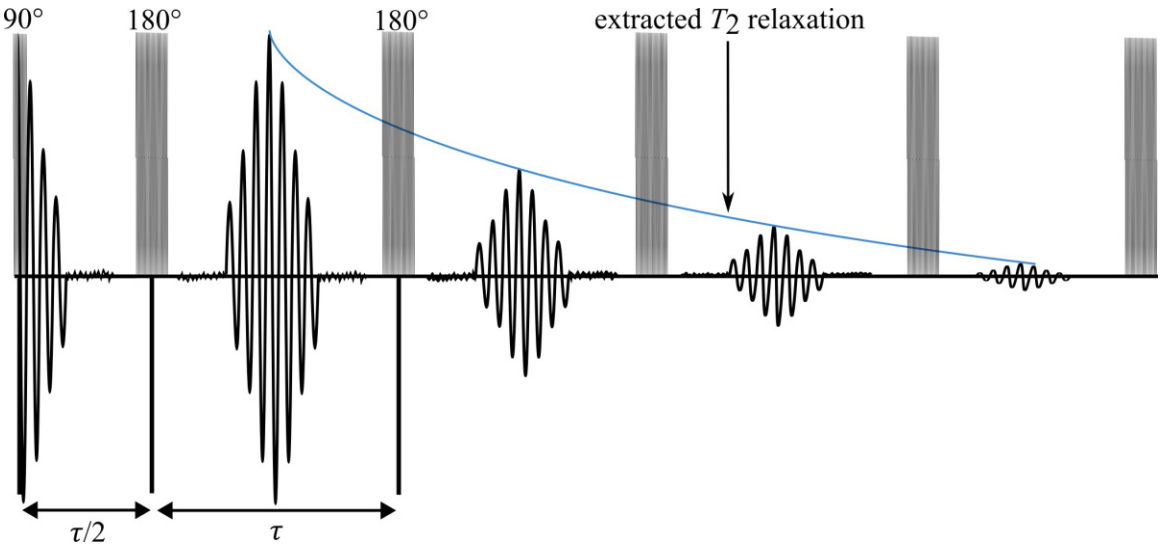

Figure 2.4: Expected response of the spin Echoes. The CPMG sequence includes a 90-degree pulse followed by a downtime $\tau/2$ then continuous 180-degree pulses followed by downtimes of τ.

Custom Electronics

Figure 2.5 shows a schematic of the developed electronics consisting of two main parts, the custom-developed control bard and the off-the-shelf PXI-based data acquisition system. On the control board, the switch is used to control the pulses that excite the sample. When the pulse generator sends a signal into the switch, the sine wave is

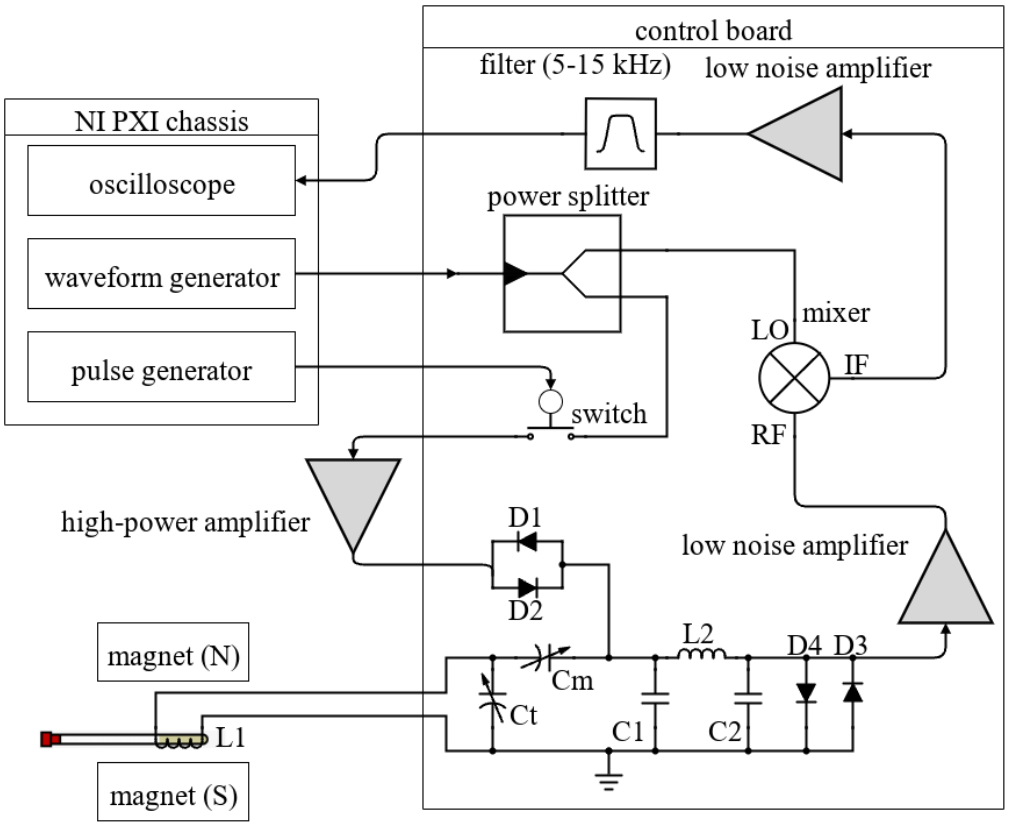

Figure 2.5: Schematic of the custom electronics used for the compact NMR system.

able to travel through the switch creating a pulsed signal. The creation of the pulsed sine wave is visualized in Figure 2.3. The signal then travels through an amplifier and into the coil. It is important to remember that this coil is where the oscillating magnetic field that creates an NMR response in the sample is generated as well as where the induced current due to the NMR response is measured. Subsequently, the resonance from the sample is directed through an additional amplifier to enhance the signal under collection. It should be noted that amplifiers with lower gain have been tested, providing mixed results. From this point, the signal is routed to a mixer to fine-tune the frequency to approximately 15 kHz, facilitating its passage through a filter and a low-noise amplifier. This sequence serves to diminish extraneous noise and unveil the distinct resonance signal. The duplexer is used to make sure only the nuclei resonance travels through the amplifier and to block any of the signals from traveling

back through the system. The voltage regulators that are used include a 12, 5, and 1.8 V regulator. These components are integrated to streamline the system into a single 24 V power supply requirement, aimed at delivering approximately 1 Amp of current. Finally, a separate impedance matching board is used for calibrating and tuning the system and is described in-depth in Section 2.5. Information about the data acquisition system can be found on the specifications sheet for the PXI-5124 digitizer. At a 50 Ω impedance, there are two filters that can be applied exclusively, a 20 MHz 2-pole Bessel filter for noise filtration and a 60 MHz 4-pole elliptical filter for anti-aliasing. As a default, only the anti-aliasing filter is on. The dynamic range at a 50 Ohm impedance varies, decreasing from 75 DBc at 0.2V to 65 DBc at 10 V [23].

Software

The software of the compact-NMR system is written in LabVIEW. The code controls the wave generation and data collection. The pulse generator functions by making an arbitrary waveform controlled by a pulse train file, turning it on and off. The sine wave generates a consistent frequency which can be set to any frequency in between 0-43 MHz. The code sets the timing and triggers to assure consistent phase of the excitation pulse. The code finally collects the data and plots the peaks of the spin echoes to produce a T_2 decay curve. A number of scans can also be set to get a higher resolution result by averaging out the results from each scan; as is typically done with this system.

Safety and Regulatory Information

As this is a magnetic resonance system, it is subject to certain US federal regulations. The frequency of this system is permitted by these regulations and the power of the system is in the range of -20 to -30 dBm depending on the specific calibration, which

is well below 1 mW. Due to this, the field strength is also well within regulatory requirements. As the system will need to be troubleshooted during operation, always ensure that the power supply is turned off when not in use. While the system operates at a maximum of 24 V, shocks are unlikely, but possible when not operating safely. According to OSHA regulations, while low-voltage systems, (typically below 50V) present a reduced risk of electric shock, they can still pose hazards such as short circuits, burns, or risks in wet environments [34].

2.3 Design files summary

Table 2.1 reports a summary of the major design files with a description provided below.

- Control Board PCB: This circuit board is the main board of the system and was developed in KiCAD.
- Impedance Matching PCB: This circuit board is used to ensure that the electronics operate at the Larmor frequency and was developed in KiCAD.
- Coil PCB: This PCB holds the coil that creates a small magnetic field to cause an NMR in the sample.
- Magnet Tray: This STEP file is for the tray that holds the coil PCB in the magnet.
- Magnet Casing: This STEP file is for holding the magnets in place during and after the construction of the magnet.
- `NMR T2 CPMG Sequence.vi`: This is a LabVIEW VI file that takes data and calculates T_2 curves.
- `NMR Single Shot Pulse Sequence.vi`: This is a LabVIEW VI file that is used for tuning the Larmor frequency.
- `7us 90 Deg-1.25 ms Tau-4 Pulses.txt`: This is a file that contains a short pulse sequence to use with <`NMR Single Shot Pulse Sequence.vi`> for Lar-

Table 2.1: Table of Design files.

Design filename	**File type**	**Open source license**	**Location of the file**
Control Board PCB	EDA file	CC BY-SA 4.0	https://osf.io/nd27h/
Impedance Matching PCB	EDA file	CC BY-SA 4.0	https://osf.io/nd27h/
Coil PCB	EDA file	CC BY-SA 4.0	https://osf.io/nd27h/
Magnet Tray	STEP file	CC BY-SA 4.0	https://osf.io/nd27h/
Magnet casing	STEP file	CC BY-SA 4.0	https://osf.io/nd27h/
NMR T2 CPMG Sequence	VI file	CC BY-SA 4.0	https://osf.io/nd27h/
NMR Single Shot Pulse Sequence	VI file	CC BY-SA 4.0	https://osf.io/nd27h/
7us 90 Deg-1.25 ms Tau-4 Pulses	TXT file	CC BY-SA 4.0	https://osf.io/nd27h/
7 us 90 Degree - 0.7 ms Tau - 5000 Pulses	TXT file	CC BY-SA 4.0	https://osf.io/nd27h/
pulse_sequence_creator_PXI5421	Jupyter Notebook	CC BY-SA 4.0	https://osf.io/nd27h/

mor frequency tuning.

- `7 us 90 Degree - 0.7 ms Tau - 5000 Pulses.txt`: This is a file that contains a long pulse sequence to use with the CPMG Sequence VI for taking data and generating T_2 curves.
- `pulse_sequence_creator_PXI5421.ipynb`: This is a MATLAB file that can be used to generate new pulse sequences.

2.4 Bill of materials Summary

A complete bill of materials is located at https://osf.io/nd27h/.

This section outlines the build instructions for the NMR system.

NMR assembly

The base NMR system is built in three stages. First, the magnet housing must be assembled which includes 3D printed parts and (1018 steel bars). Second, the PCBs must be assembled with the proper electronic components. Third, the system needs to be calibrated to the correct frequency.

Tools used for the construction of the package include the following:

- Soldering iron
- Sn60/Pb40 22 gauge solder
- Sn63/Pb37 solder paste
- Flathead screwdriver
- Pliers
- Razor blade
- Instant glue (i.e. Cyanoacrylate Adhesive or Super Glue®)
- Clamps
- Wood slats

Other optional tools

- Re-flow soldering bed

Building the magnet

HANDLE MAGNETS WITH EXTREME CAUTION! KEEP AWAY FROM METAL OBJECTS AND OTHER MAGNETS. GLOVES HIGHLY ENCOURAGED

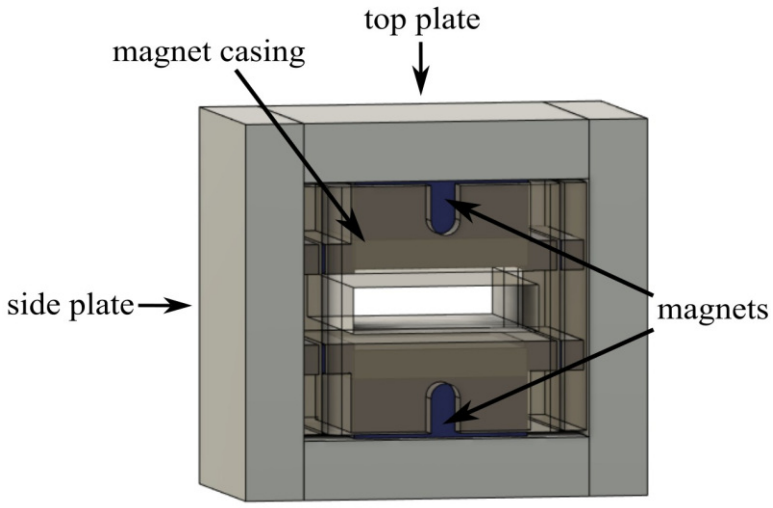

Figure 2.6: Fully assembled magnet.

The process for building and assembling the main magnet shown in Figure 2.6 is described in the enumerated steps below.

1. Obtain materials in Table 2.2. Figure 2.7 presents an image of these components.
2. Once materials for the magnet have been obtained, it is time for assembly. Figure 2.8 provides an overview of the correct polarity orientation of the main and aliment magnets. Refer to Figure 2.9 and Figure 2.10 for visualizations. ****Reminder magnets are extremely dangerous and need to be handled with planning and caution.****
3. For sub-assembly a (Figure 2.9(a)), begin by attaching the main magnets to steel magnetic caps (make sure each sub-assembly a has opposite polarities using a Guassmeter). Next, attach the main magnets with steel to the center of each top plate. It is best to use layers of non-magnetic slats (such as wood or plastic) in between the magnets and steel to avoid sudden attraction that

Table 2.2: List of parts required for magnet assembly.

Amount	Description	Part Name	Location
1X	3D printed magnet casing	magnet casing	https://osf.io/nd27h/
2X	3D printed magnet aligner	magnet aligner	https://osf.io/nd27h/
2X	1018 carbon steel $12.7 \times 50.8 \times 64$ mm	top plate	bill of materials
2X	1018 carbon steel $12.7 \times 50.8 \times 80$ mm	side plate	bill of materials
2X	1018 carbon steel $38.1 \times 38.1 \times 6$ mm	magnet cap	bill of materials
2X	BX8X88 magnet	main magnet	bill of materials
8X	BX844 magnet	alignment magnet	bill of materials

could lead to damage to the magnet or injury to yourself. Slowly remove layers of non-magnetic slats until the magnet is flush with the steel.

4. To begin assembling sub-assembly b (Figure 2.9(b)), instant glue the magnet aligners to the center of each side plate with the magnet slots parallel to the short edge of the side plate and put them aside for later.
5. Next for sub-assembly b, take two of the alignment magnets and insert them into each of the magnet holders. Make sure to pay attention to the polarity of the magnets using a Gaussmeter and follow the polarities shown in Figure 2.8. Note that the Guassmeter's probe needs to stay in the same orientation while measuring polarity as it will cause the reading to change signs if the opposite side of the probe is used.
6. Next insert sub-assembly a into one side of the magnet casing. Make sure the steel bar is flush with the top of the magnet casing. Refer to Figure 2.10.
7. Carefully insert the second sub-assembly a into the other side of the magnet casing.

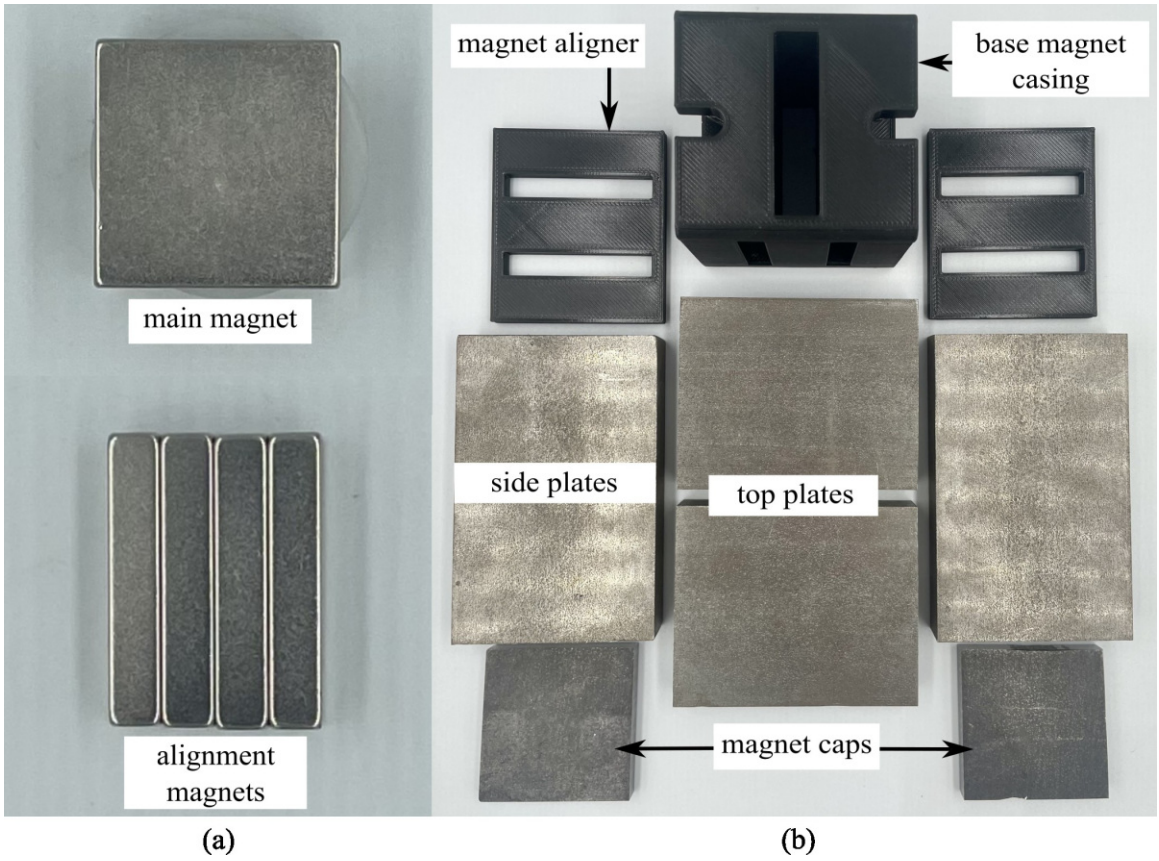

Figure 2.7: Constituent parts for the magnet assembly, showing: (a) magnets, and (b) steel field guides and plastic component holders.

8. Once the magnets are correctly positioned and the polarities are in the correct orientation, carefully bring the first sub-assembly b edge in contact with the ends of the top plates and slowly let it become flush with them. Note that this side should have a very strong attraction to the center of the magnet and should go on easily with the magnets in the correct polarity.
9. Take the second sub-assembly (b) and bring it into contact with the other ends of the top plates. This time, applying force will be necessary to ensure it is flush and securely attached to the rest of the magnet, provided the polarities are correctly aligned.
10. Measure the inductance of the assembled magnet. This value should be close to 0.56 Tesla. Refer to Section 2.5. If the value is measurably less than 0.56

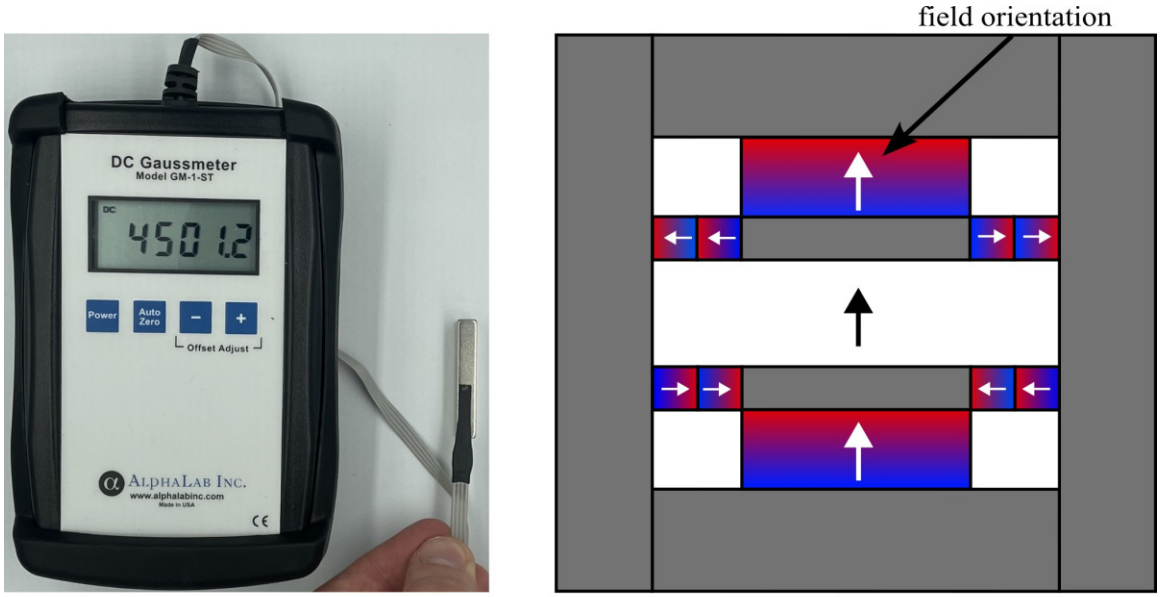

(a) (b)

Figure 2.8: Measuring magnet polarity, showing: (a) Gaussmeter measuring an alignment magnet in the positive magnetic field orientation, and (b) a diagram showing polarities of the magnetic assembly.

Tesla, then the polarity orientation of the magnets may be incorrect.

Assembling the PCB

This section outlines the detailed procedure for assembling the printed circuit boards (PCBs) critical for the NMR system's operation, ensuring the correct order of component placement/soldering is essential as the duplexer should not be installed till calibration is complete. The assembly steps are:

1. Begin by obtaining the NMR Control Board, Impedance Matching, and Coil PCBs provided from the Electronic Design Automation (EDA) files in the design files summary.
2. Obtain the SMD components including the Mixer, Switch, Power Splitter, Low Noise Amplifier, 1.8 V regulator, 5 V regulator, 12 V regulator, Charge Pump Converter, Resistors, and Capacitors. Values are listed on the PCB. Specific parts can be found in the bill of materials Section 2.4.

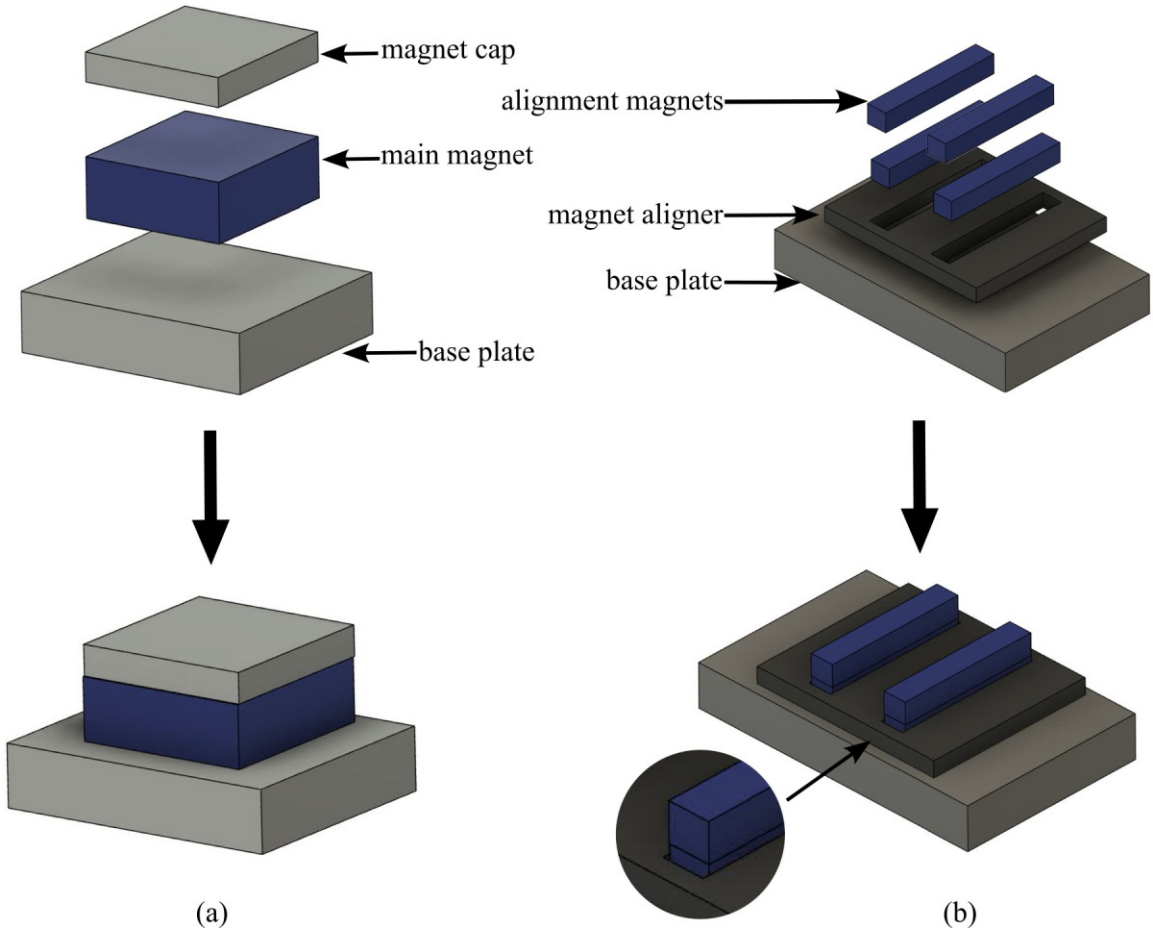

Figure 2.9: Magnetic component assembly, showing: (a) construction of sub-assembly a the top plate to the main magnet and steel magnet cap, and (b) sub-assembly b gluing the magnet aligners to the side plate and inserting the alignment magnets.

3. Start by soldering the SMD components on the Control board, excluding those in the duplexer section (the diodes, inductor, and two capacitors). This does include the surface mount SMA connectors. Apply solder paste and place the components on their respective pads. Use a reflow soldering oven set to 400-425°C or an equivalent method. Avoid using a heat gun as it may melt and damage the components. Ensure that you follow the resistor and capacitor values marked on the board. Refer to Figure 2.11 for the correct orientation of components, where dots on each component indicate pin 1.

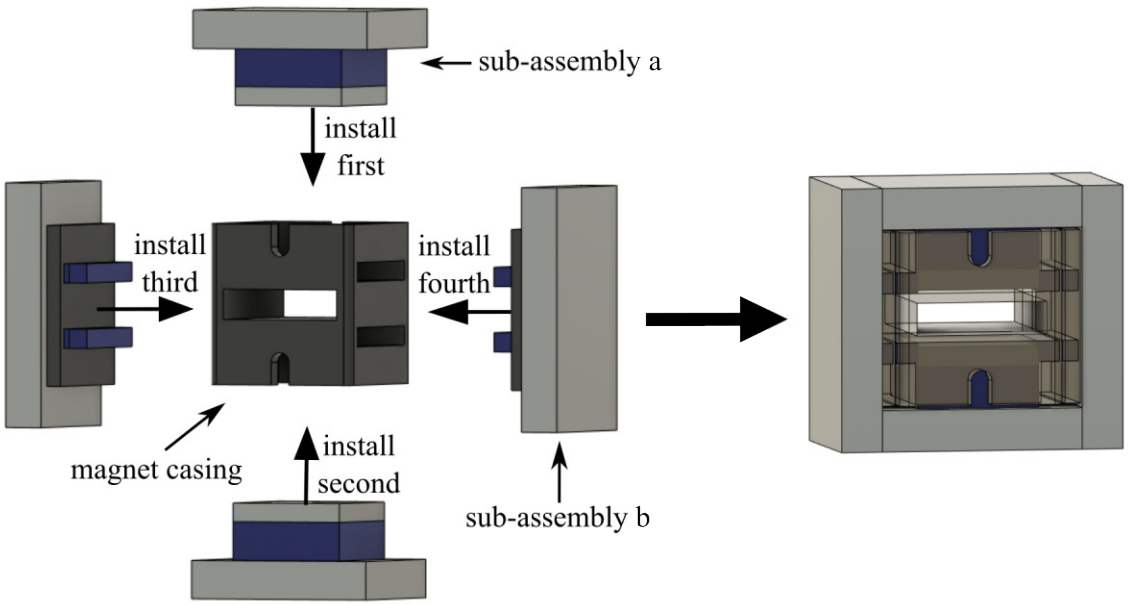

Figure 2.10: Magnetic assembly, showing the order of operations for adding the side assemblies to the plastic frame.

4. Next, solder the through-hole SMA connectors to the board.
5. Once soldering is complete check for continuity and shorts between the pins of each component. To check for continuity, follow the traces on the PCB denoting wires from component to component. Grounded vias are present throughout the board to aid in checking for shorts.
6. The next step is assembling the coil PCB. To accomplish this, utilize a cylinder (such as a screwdriver) with a 5 mm diameter, matching that of the glass tube, take 140 mm of copper wire, and precisely wind the wire around seven times. It is essential to maintain a tight wire, minimizing any gaps between each coil. Tweezers can be employed to achieve this desired outcome, followed by the utilization of instant glue to secure the coil in place. Refer to Figure 2.12(a) for the final outcome.
7. Moving on to the impedance matching board, solder the variable capacitors and SMA connectors to their respective holes. Figure 2.12(b) shows completed PCB.

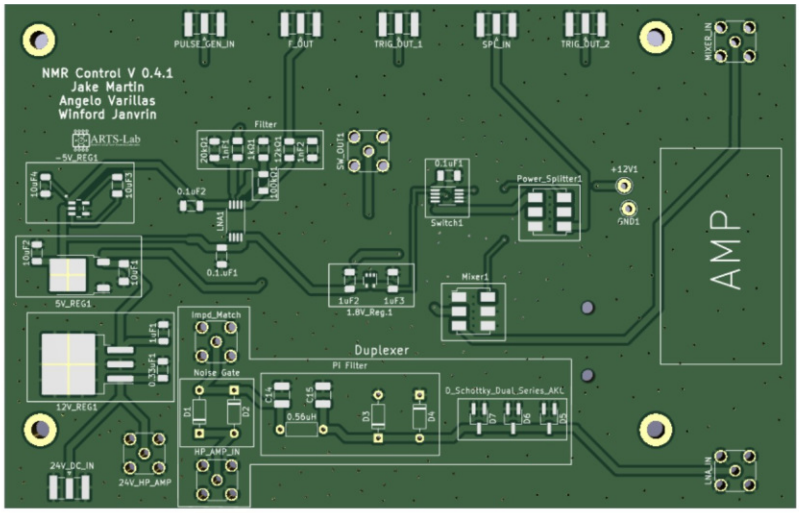

(a)

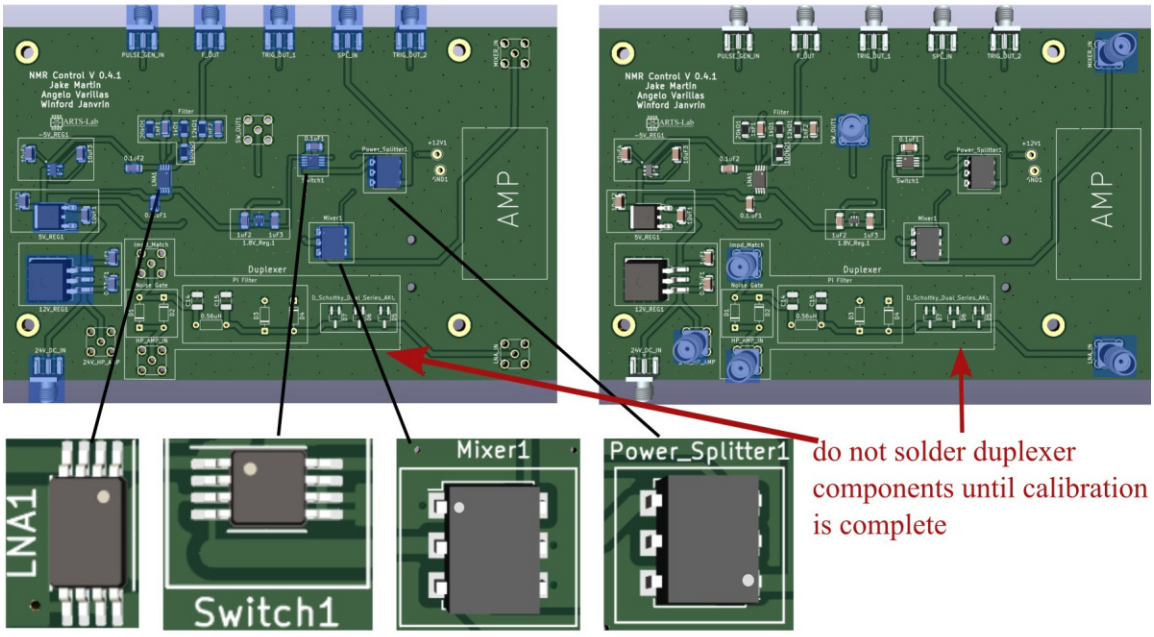

(b) (c)

Figure 2.11: Control board PCB assembly, showing: (a) control board, (b) soldered SMA components including orientation of components, and (c) soldered through hole components.

8. Once the instant glue has set and the coil is finished solder the two ends onto the PCB.
9. Lastly is the duplexer section of the Control PCB, this board requires calibration so follow the steps in order. First solder the SMA connectors and the inductor (0.56 μH) to their respective spots. Once done Move to Section 2.5 to finish

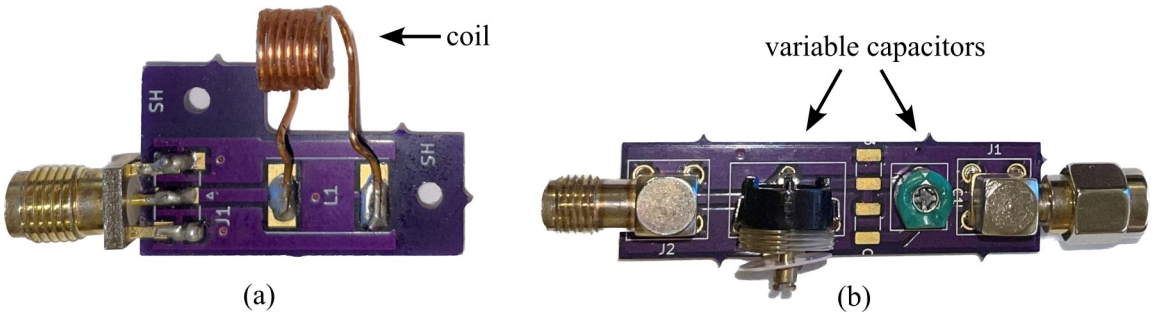

Figure 2.12: Component sub-boards, showing: (a) coil PCB. (b) populated impedance matching PCB.

calibrating and soldering of the PCB.

Probe Calibration

This section is for calibrating the coil/probe and pi filter using the impedance matching and Duplexer boards. Note this only needs to be done once during assembly but can also be used for troubleshooting the system. The steps to calibrate the probe are:

1. Begin by acquiring a Gaussmeter. Once acquired, measure the inductance of your magnet by inserting it at the very center (refer to Figure 2.13). Record the highest value in Tesla.
2. To calculate the Larmor frequency (ω_0) of your magnet use the following equation

$$\omega_0 = B_0 \cdot 42.58, \tag{2.1}$$

   where ω_0 is the Larmor frequency in MHz, B_0 is the magnet inductance in T and 42.58 is the gyromagnetic constant for hydrogen in MHz/T. The result should be in the low to mid 20 MHz. (Our Larmor frequency was 24.2 MHz)
3. With this Larmor frequency we are now able to calculate an approximate capacitor value for the duplexer. Since this is an LC circuit, the angular frequency

Figure 2.13: Recording magnet inductance using a Gaussmeter.

of the circuit can be found using:

$$\omega_0 = 1/\sqrt{LC}. \tag{2.2}$$

Solving for C results in:

$$C = \frac{1}{(f_0 \cdot 2\pi)^2 \cdot L}, \tag{2.3}$$

where C is the capacitance value in F, f_0 is the Larmor frequency in Hz, and L is the inductance value in H. Here, the extra factor of $1/(2\pi)^2$ comes from the Larmor frequency being used as the linear frequency of a sine wave in the LC circuit. The calculated capacitance value should be between 65 pF and 85 pF. Since every magnet won't have the exact same frequency, this is reported as a range. Additionally, the measured calibration can differ from this ideal calculation. In testing, C15 controlled the center frequency of calibration and C14 helped to regulate ripple. For this system, C15 was 60 pF and C14 was 68 pF.

4. Solder calculated capacitors to the duplexer board.

5. Obtain a spectrum analyzer and a BNC 50 Ω feed-through terminator to use for the calibration.
6. Connect the tracking generator source to the RF input.
7. Turn on the spectrum analyzer and go to the tracking generator menu. In the menu set the level to -20 dBm.
8. Open the frequency menu and set the center frequency to the calculated Larmor frequency.
9. Open the span menu and adjust the span to 30 MHz.
10. Connect the Imped Match SMA on the NMR Control Board to the spectrum analyzer. A dip should appear near the Larmor frequency of the magnet. If the dip is not within +-1 MHz of the frequency then a different capacitor value will need to be chosen and soldered on the board. This will need to be repeated until this criteria is met.
11. Once the duplexer is properly calibrated, solder on the diodes. This will complete the control board represented in Figure 2.14.

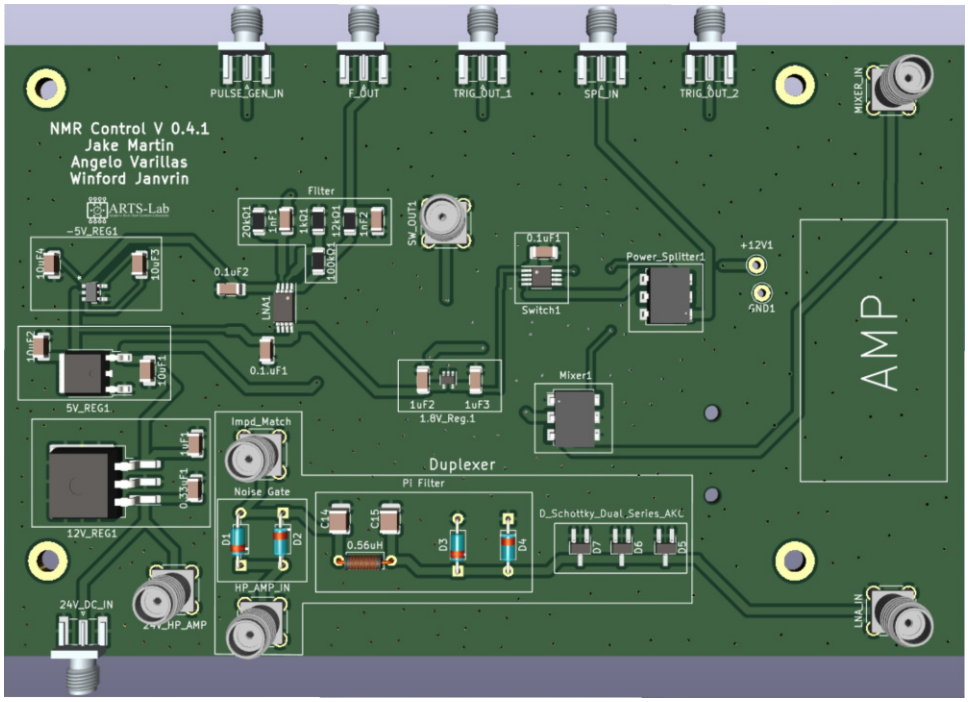

Figure 2.14: Completely populated control board.

12. Next, the impedance matching board and coil will be calibrated. Refer to Figure 2.15 and Figure 2.16 for visuals.

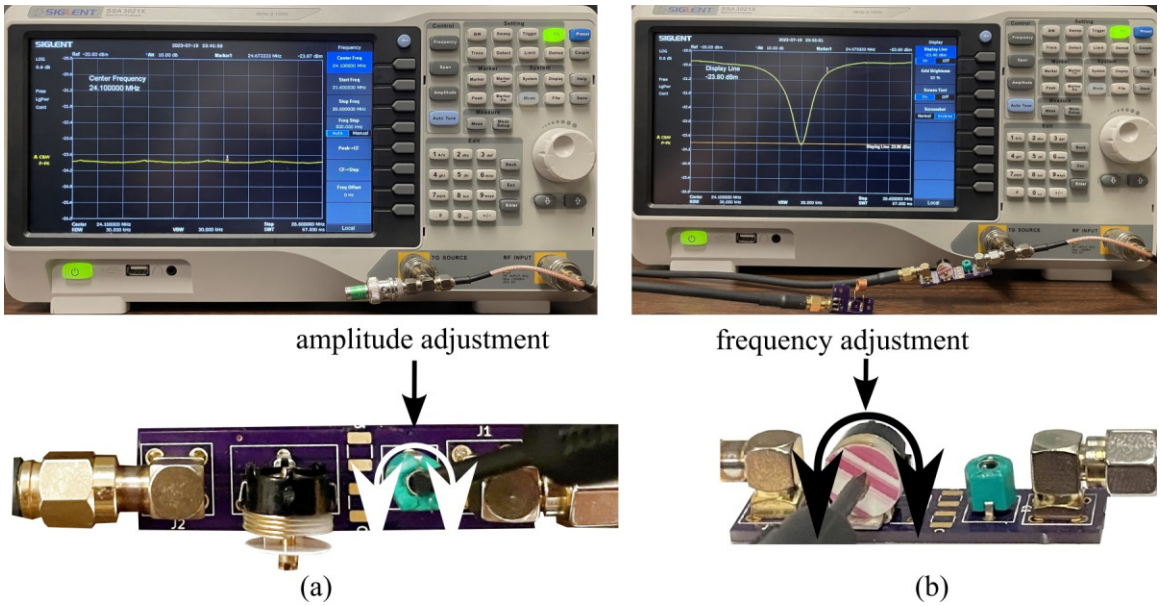

Figure 2.15: Calibration of the probe, showing: (a) setting the display line at 50 Ω feed-through terminator signal and (b) properly calibrated impedance matching board and coil.

13. Continue by opening the amplitude menu and setting the reference to -20 dBm and the scale to 0.6 dB.
14. Open the span menu and set the span to 5 MHz.
15. Plug in the 50 Ω feed-through terminator.
16. Create a display line over the signal that will be used as a reference later.
17. Connect the impedance-matching PCB to the coil PCB using a male BNC cord. Note that changing this chord later can affect the calibration. It should be noted that the specific variable capacitors are intended to be used with cords between 6 and 30 in. Cord lengths outside this range will require different variable capacitors. It is also important to use a high-quality cord for this. The bending of the cord during calibration and in the fully assembled system will be different, causing calibration issues with low-quality cords.
18. Now remove the 50 Ω feed-through terminator and attach the impedance-

matching PCB with the coil PCB. A dip should be visible on the screen.

19. Use a small flathead screwdriver to adjust the variable capacitors until the very center of the dip is at the Larmor frequency and touching the reference display line.

Final Assembly

This subsection provides a comprehensive guide for the final assembly process of the NMR system, detailing the integration and connection of all components to ensure operational readiness for field deployment.

1. To begin the final assembly first acquire an NI PXIe chassis or equivalent system for waveform generation and data collection. There are a number of PXI cards available form National Instruments or other vendors that could be used for this purpose. In general, this hardware requires a digitizer and two independent channels of arbitrary waveform generators (AWG).
2. Using hardware available to the authors, a PXIe-1083 chassis and three PXI cards were used (note that equivalent cards could be used), they are:
    - NI PXI-5124 150 MHz, 200 MS/s, 12-Bit, 2 channel, 8 MB/channel, PXI Oscilloscope
    - 2X PXI-5421 43 MHz, 16-Bit, 1 Channel, PXI Waveform Generator
3. Insert the cards and plug a thunderbolt cable from the computer into the chassis card.
4. The last step is wiring all the parts together. This will be done mainly with SMA, SMB, and BNC cables. Refer to Figure 2.17

    All parts can be found in the bill of materials. Parts needed at this stage will be:
    - Assembled PCB's

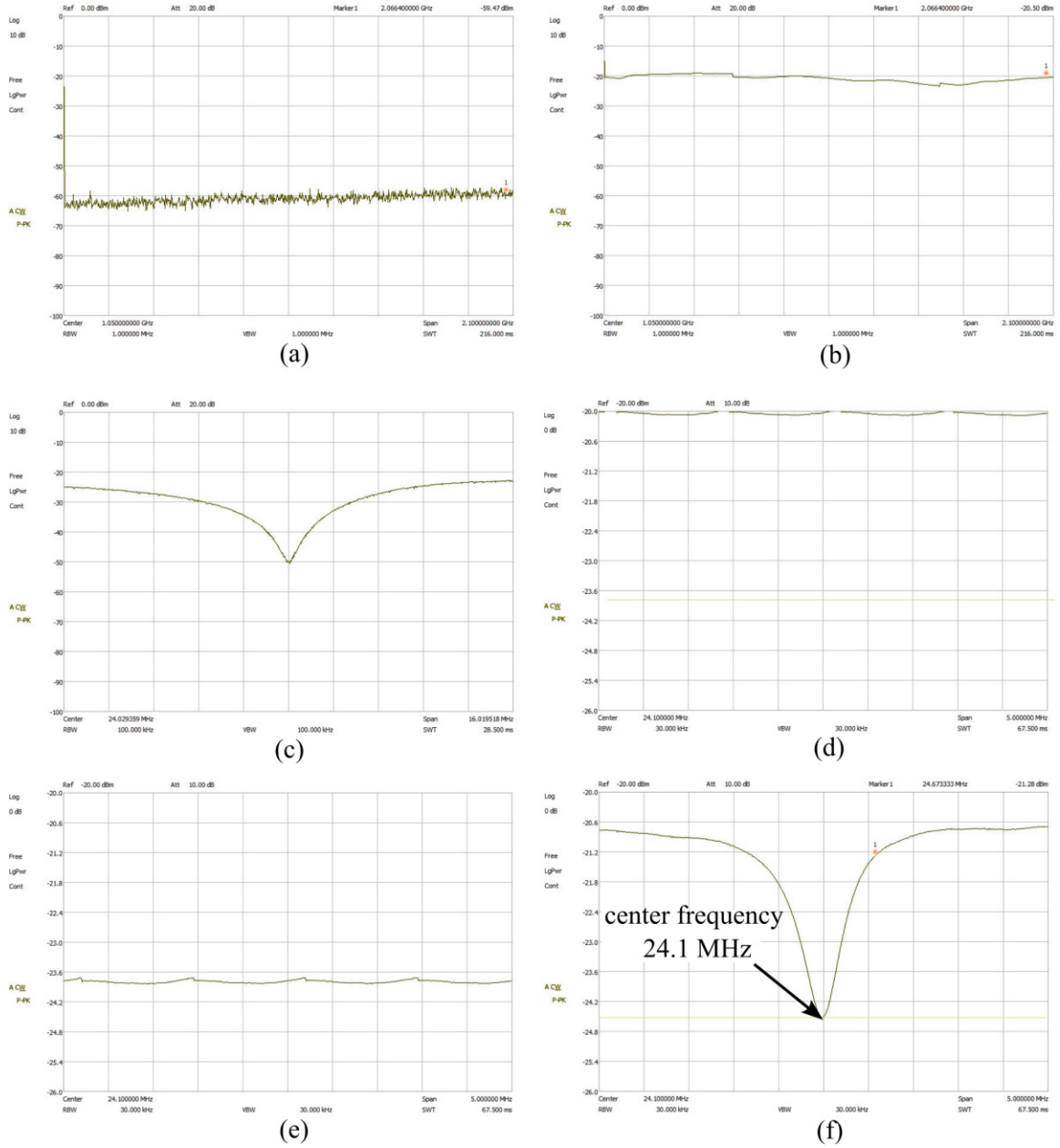

Figure 2.16: Spectrum analyzer setup and calibration of impedance matching board and duplexer showing: (a) spectrum analyzer default settings, (b) tracking generator setting turned on and level set to -20 dBm, (c) frequency adjusted and calibrated duplexer board connected, (d) frequency, span, and amplitude settings adjusted to calibrate impedance matching board, (e) 50 Ω feedback terminator connected to create reference line, and (f) properly calibrated impedance matching board connected to spectrum analyzer and coil PCB.

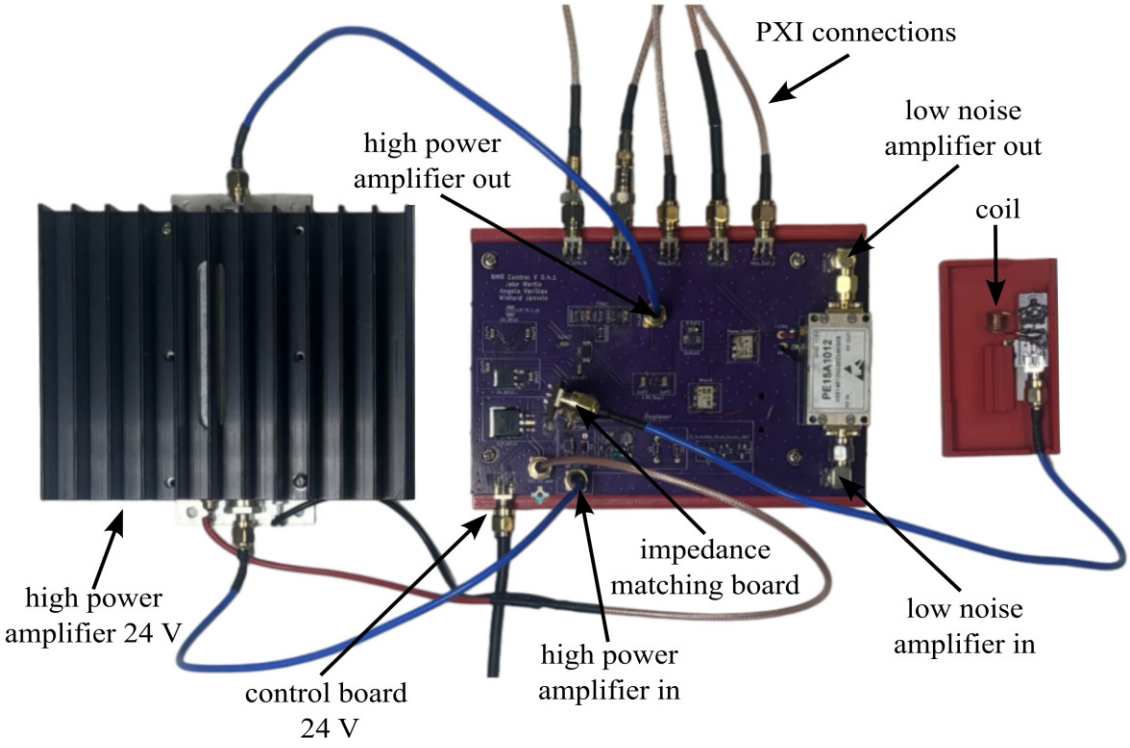

Figure 2.17: Completely populated control board with wiring.

- Magnet
- 24 V DC power supply
- RF power amplifier
- Low-noise amplifier (LNA)
- PXI Chassis with cards
- 3X male SMA cables
- 3X female SMB to male SMA cables
- 2X power and ground to SMA connector
- 2X BNC to SMA cables
- 2X Male Pin SMA adapter (right angle)

5. To start connect male pin SMA adapters (right angle adapters) to both sides of the low noise amplifier then screw the *RF IN* side into the *LNA_IN* port and

the *RF OUT* side into the *MIXER_IN* port.

6. Next solder a wire for both power and ground from the control board to their respective pins on the amplifier.
7. Wire the control board to the NI card using the SMA to BNC and SMA to SMB cables. Refer to Figure 2.18.

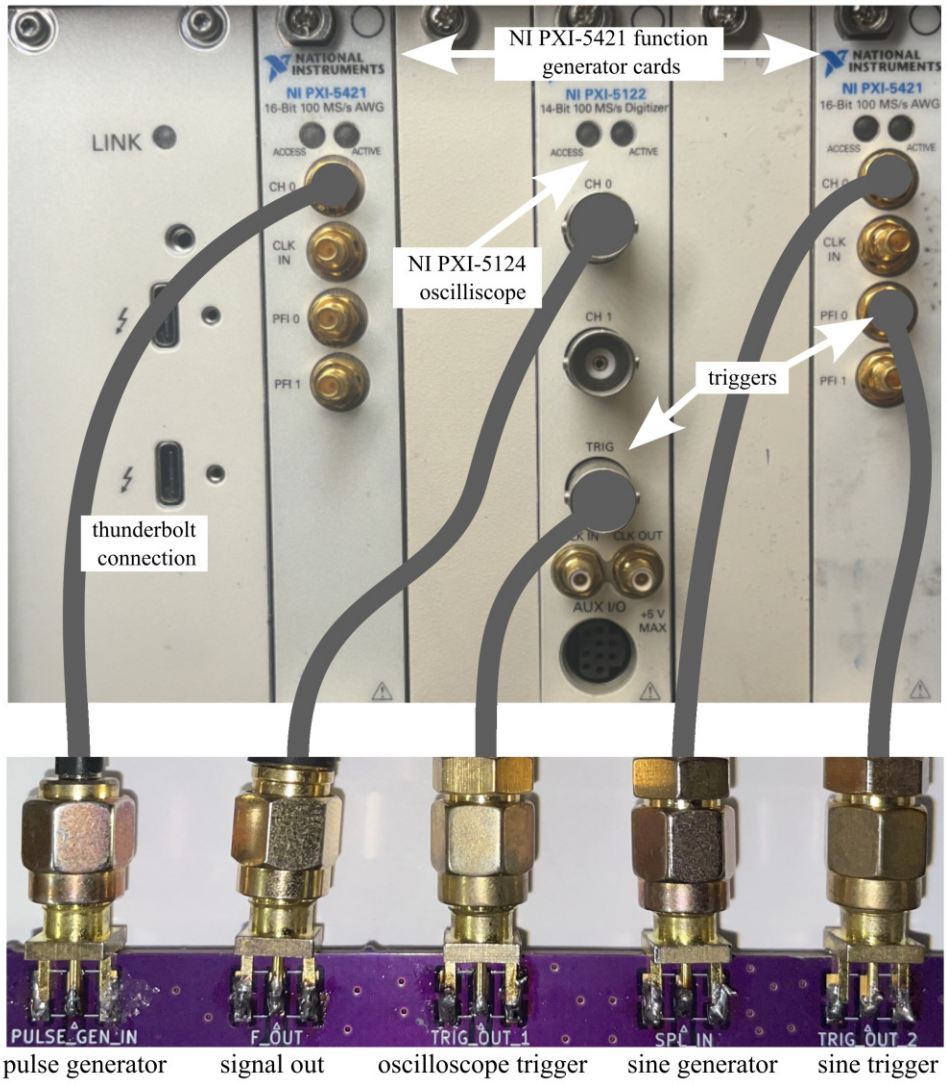

Figure 2.18: Wiring diagram from the PXI cards to the control board.

8. Now that everything is connected correctly, obtain the magnet tray found in the Design files summary section. This tray is used to hold the coil PCB at the center of the magnet where the signal will be at its strongest.

9. Insert the coil PCB into the magnet tray, ensuring that a sample can easily slide into the coil. See Figure 2.19.
10. Now slide the tray into the magnet.

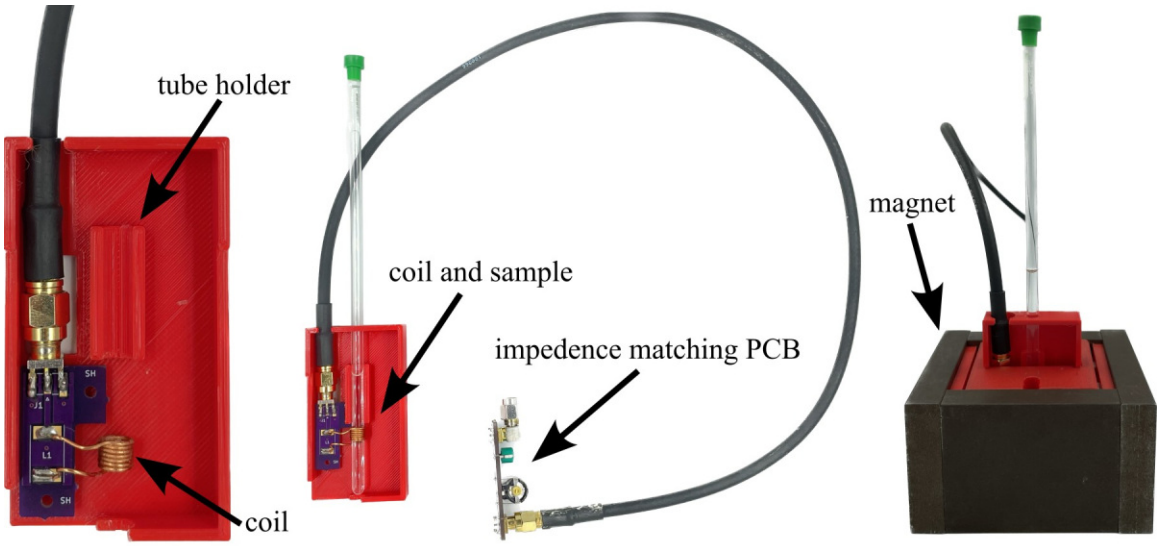

Figure 2.19: Details of the sample tube and coil tray, showing: (a) insert the coil PCB into the magnet tray; (b) complete assembly of coil and tray with sample, and; (c) tray with sample inserted in magnet.

11. Connect the impedance matching PCB to the port labeled *Impd_Match* on the control board.

2.6 Operation instructions

This section outlines the operation instructions for the NMR system.

Software Interface

All LabVIEW code is provided in the repository and its setup process is critical for operating the compact NMR system effectively, allowing users to control and monitor the performance of the NMR experiments. The setup involves configuring the software

to interact with the hardware setup described in previous sections, specifically the PXI cards required to interact with the NMR pulse sequences. The detailed steps:

1. Begin by turning the PXI chassis on and turning on the control board's power supply.
2. Open <`NMR Single Shot Pulse Sequence.vi`> in LabVIEW. The single shot pulse sequence is used for calibrating the system because you can quickly test for a signal.
3. Once open, in the front panel of LabVIEW enter the Larmor frequency for your system and open <`7us 90 Deg-1.25 ms Tau-4 Pulses.txt`> in the pulse train file section.
4. Run the system. Your results will probably look like one of these:
    - If everything is perfect the results should look similar to those in Figure 2.20. If this is the case you can move on to Section 2.6 and skip the following steps.

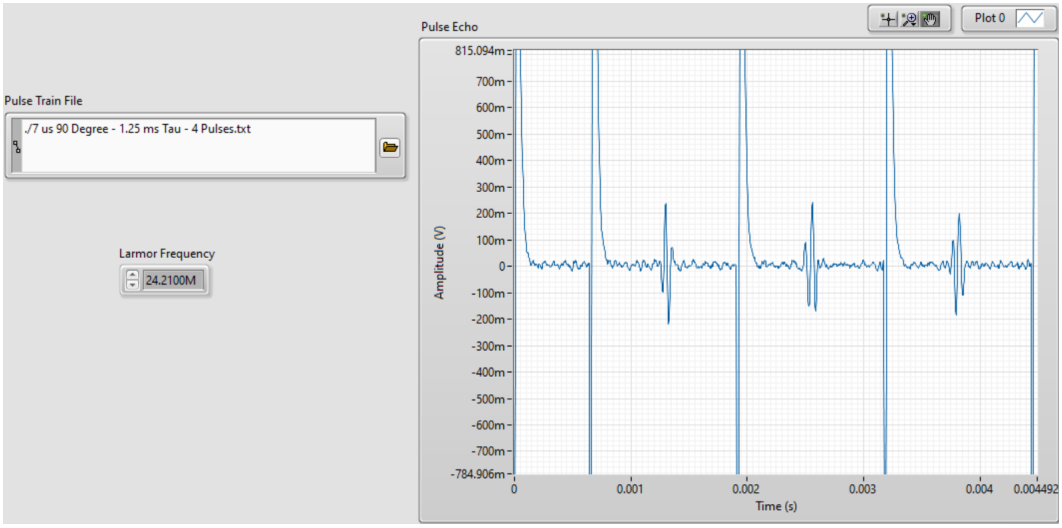

Figure 2.20: NMR single shot pulse sequence with a strong signal.

- If the system is set up correctly but the Larmor frequency is not precise the results could look similar to those in Figure 2.21. If this is the case adjust the Larmor frequency in LabVIEW by small intervals until you pick

up a signal. It is best practice to use coarse adjustments of 0.01 MHz and fine adjustments of 0.001 MHz. Wait approximately 10 seconds between frequency adjustments to allow the nuclei to fully relax before testing again. If the signal is unobtainable re-calibration of the probe may be necessary.

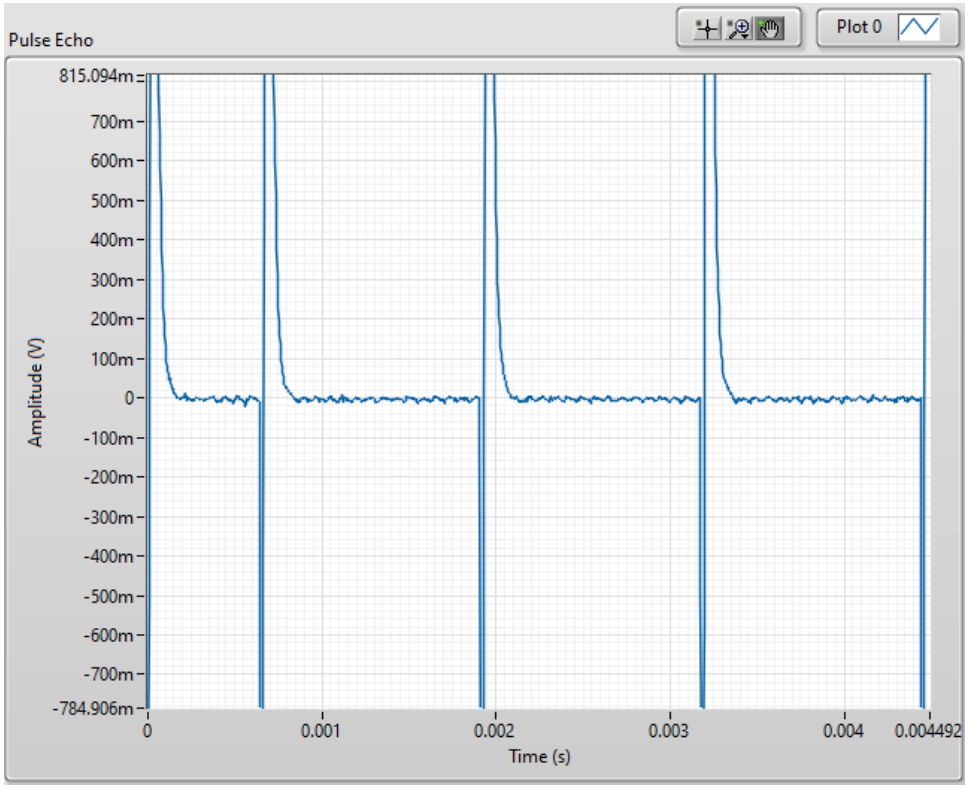

Figure 2.21: NMR single shot pulse sequence with no pulse resonance

- If a component is not plugged in properly or lacks proper continuity in the system, you will likely see a flat line as shown in Figure 2.22. Note that not only is there no signal, but also a DC offset. This will only happen if power is off or the system lacks proper continuity. To solve this problem, first, ensure that everything is correctly connected and that the power supply is turned on. An easy mistake that could cause improper connections is by putting two cords channels on the NI PXI-5124 or the NI PXI-5421 rather than one cord on a channel and one on a trigger. Refer to Figure 2.18 for the proper connections. If the issue persists, proceed with

these troubleshooting steps:

- Check if the coil has been pushed up or down. If so, push it so that it lies inbetween the solder points
- Check to be sure the tray is properly placed in the magnet
- Check to be sure the sample in the tube is within the bounds of the coil
- Check to be sure all SMA cables are tightened as needed
- If the issue persists after these steps, it is likely that even though all wires are tightened, there is an incomplete connection somewhere. In this case, remove all wires and redo the wiring

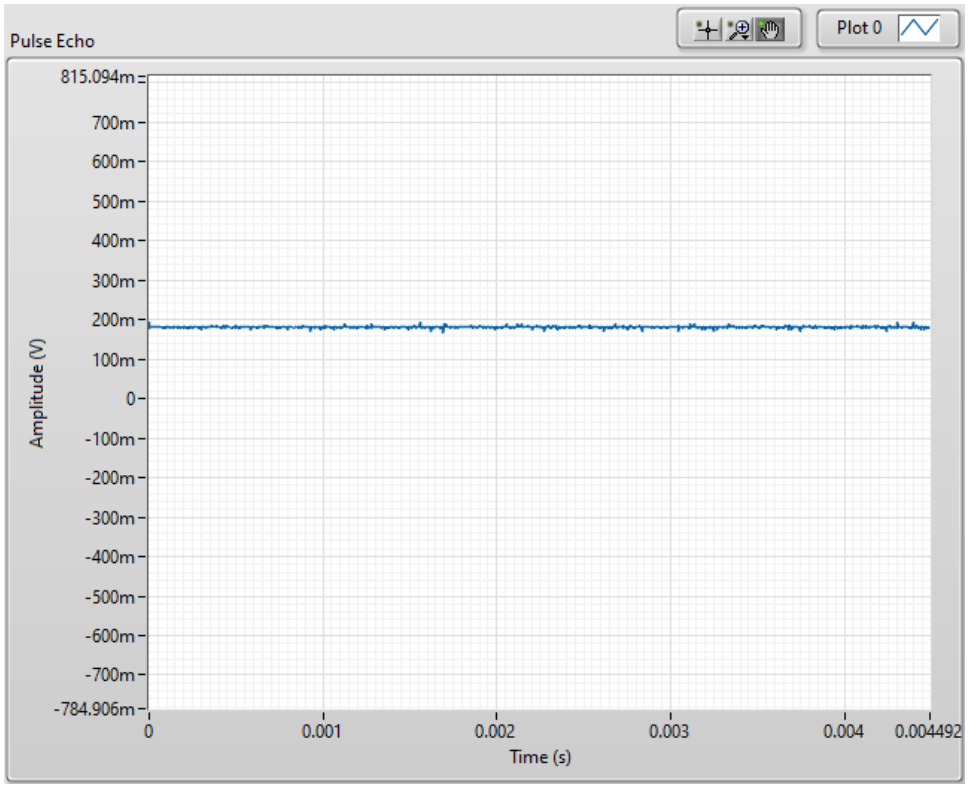

Figure 2.22: NMR single shot pulse sequence with no signal.

Running a test

This section outlines the steps for conducting a test run using <`NMR T2 CPMG Sequence.vi`>. This program is designed to evaluate the functionality of the compact NMR system. Follow these instructions to configure the sequence parameters, execute multiple scans, and assess the system's performance through visualized results.

1. Open <`NMR T2 CPMG Sequence`> in LabVIEW.

2. In the front panel of LabVIEW enter the Larmor frequency for your system and open <7 us 90 Degree - 0.7 ms Tau - 5000 Pulses.txt> in the pulse train file section.

3. Choose the number of scans you want the system to collect up to 8 (resolution increases with the number) and hit run.

4. If the system was properly calibrated and the single shot results were strong the results should look similar to Figure 2.23:

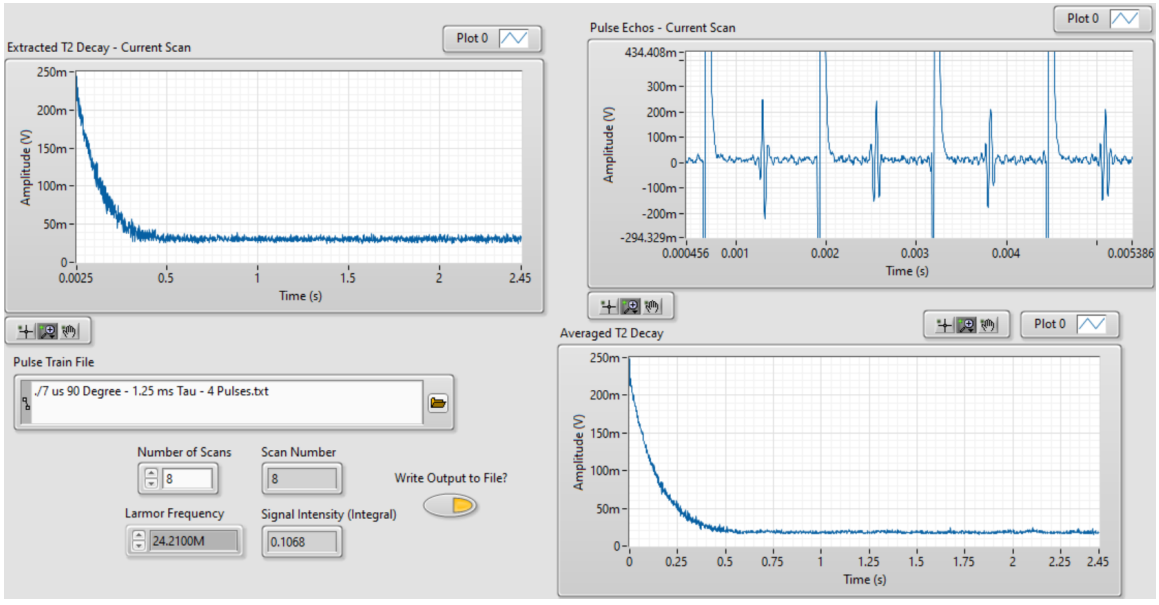

Figure 2.23: NMR T_2 CPMG Sequence results

Note that other CPMG pulse sequences may be useful for different applications. The pulse sequence files mentioned in this paper were generated using< `pulse_sequence_creator_PXI5421.ipynb`>. This Matlab program can be used to generate new pulse sequences for different pulse lengths and values of τ. The optimization of pulse sequences is left to the reader to allow for tuning of the pulse sequences to their measurement goals and hardware.

2.7 Validation and characterization

The accuracy of the compact TD-NMR system was tested in the copper T_2 relaxation study discussed here. Copper solutions were prepared by dissolving Copper Sulfate in deionized water resulting in concentrations ranging from 0 to 200 ppm of Copper(II) sulfate. These solutions were placed in 5 mm diameter test tubes so that the sample could be placed in the magnet tray and maintained at a centered position in the magnet. To maintain consistent data throughout measurements, the placement of the tube in the coil and magnet must remain constant, highlighting the importance of the magnet tray.

Each measurement consisted of four NMR scans that detect pulse echos over a 3.5 second window. The maximum value of each spin echo is read and after the scan is complete, the maxima are plotted with respect to time, resulting in a T_2 curve. Each measurement takes the mean of the four T_2 curves from the scans, resulting in one set of data per measurement. Every concentration of copper was measured three times with this criteria. Using a non-linear least squares fit to Equation 1.8, we acquired T_2 times and fitted T_2 curves for each of the samples. The fitted data for these curves can be seen in Figure 2.24.

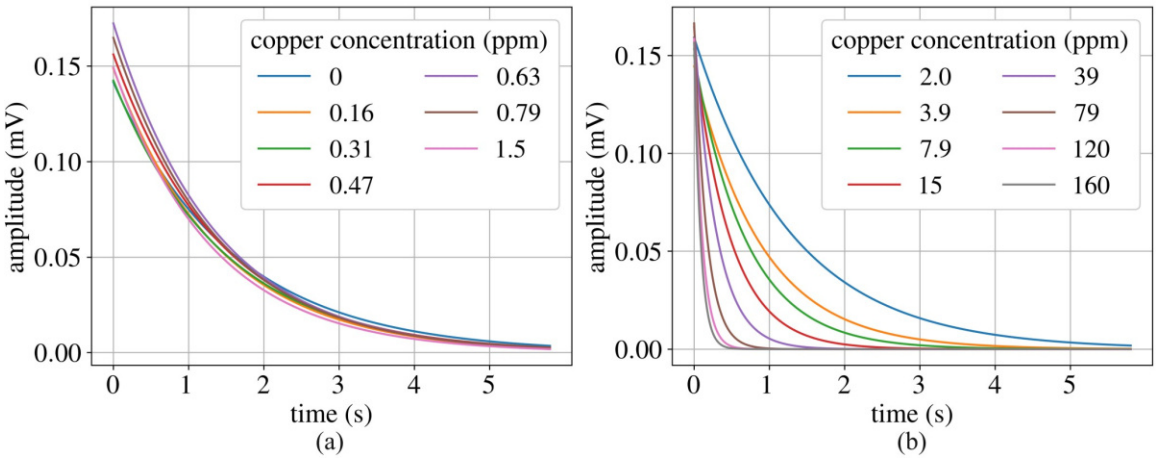

Figure 2.24: Fitted data showing the T_2 curves for varying concentrations of dissolved copper, showing: (a) ppm from 0 to 1.5 ppm and (b) ppm from 2 to 160 ppm.

After collecting the T_2 times for each copper sample, the relationship between copper concentration and T_2 time was examined. It has been shown previously that increasing copper concentration in a fluid leads to a decrease in T_2 time [1]. Figure 2.25 shows the relationship measured between T_2 time and copper concentration in ppm, highlighting an agreement with the previous study. Furthermore, within three standard deviations, the system is capable of measuring concentrations of copper dissolved in deionized water of around 900 ppb. The deionized water was purified using a Milli-Q water purification system (i.e. MQ water).

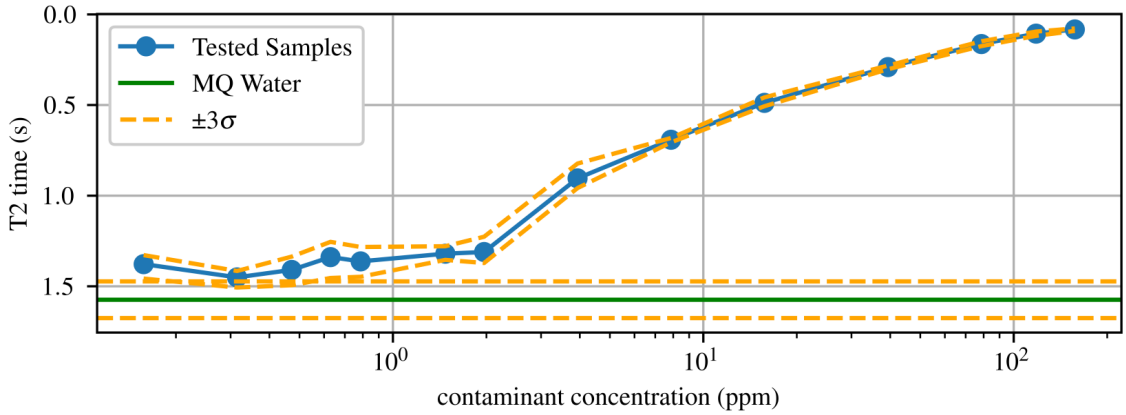

Figure 2.25: Copper T_2 time with varying concentration.

This brief T_2 relaxation study showcases the TD-NMR system's ability to measure

pollutants in water systems by comparing the T_2 curves to those of water.

While this NMR system is capable of distinguishing copper-saturated water from deionized water at concentrations up to 900 ppb, there are some limitations to what can be measured. Since this is an (^{1}H) NMR system, it can only detect molecules bonded with Hydrogen like fuels and oils as well as materials that affect Hydrogen magnetically, such as paramagnetic materials like copper ions. It is unable to detect ions like aluminum and zinc that are dissolved in water, unless something else is added that allows Hydrogen to bond with them. Some current limitations for the system include performance under temperature variability and the need to test deionized water as well to be a baseline for the measurement.

To test the temperature variability of the system, the magnet was cooled and heated to 10 and 33 °C respectively while both the amplitude of the signal and the Larmor frequency were measured. In this range, the signal strength of the magnet remains constant within error, but the Larmor frequency varies. Because of this, if the system were to be deployed in-situ, either temperature control, automated Larmor frequency tracking, or a combination of both would be required. Figure 2.26 shows the results from this exploration.

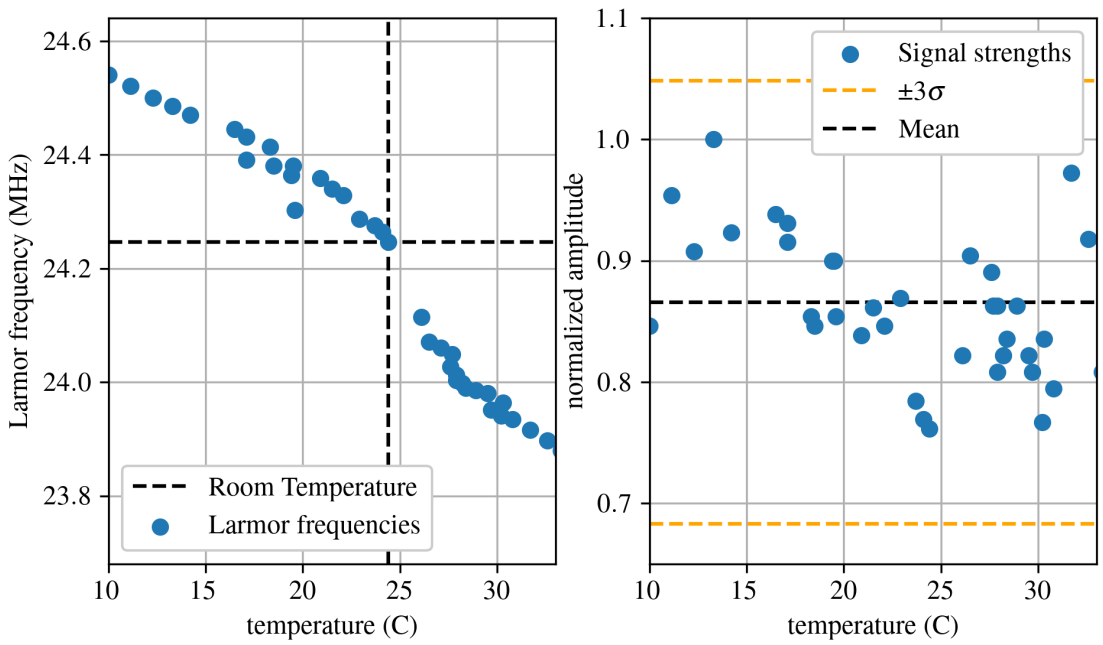

Figure 2.26: Temperature variance of the system showing: (a) how the Larmor frequency changes due to changes in the magnet's temperature and (b) how the initial signal strength changes due to changes in the magnet's temperature.

Overall, this chapter introduced a Hydrogen-based NMR system capable of detecting copper contaminated water at concentrations at and above 900 ppb. While this is an effective tool capable of being adapted for in-situ remote observation, in this chapter, only a desktop version of the system has been discussed. In order to adapt this system for remote observation, there are several things that must be adjusted such as temperature control and the ability to collect data without the presence of a researcher. Chapter 3 discusses how these problems were solved, introduces an adaptation of this system capable of remote data collection, uses that system to take data at Rocky Branch Creek in downtown Columbia, SC, and uses that data in conjunction with data taken on different concentrations of Cu(II) contaminated water in order to develop a machine learning model capable of estimating and predicting the Cu(II) concentration of creek water.

Acknowledgments

This material was sponsored by the Army Research Office (ARO) under Grant Number: W911NF21-1-0306 and the National Science Foundation (NSF) under Grant Nos. 2152896 and 2344357. Additional support was also provided by the University of South Carolina through grant number 80004440. The views and conclusions contained in this document are those of the authors and should not be interpreted as representing the official policies, either expressed or implied, of ARO, NSF the U.S. Government, or the University of South Carolina. The U.S. Government is authorized to reproduce and distribute reprints for Government purposes notwithstanding any copyright notation herein.

Chapter 3

Continuous Water Quality Monitoring using Field Deployable NMR and Explainable AI

[1] This chapter reports on the development of a temperature-controlled time-domain NMR system with the capability of being deployed to rivers and creeks to monitor water quality in-situ. To do this, a machine learning approach utilizing random forests is trained on water quality and NMR data from copper and iron-contaminated water, tested using in-situ water quality and NMR data from creek water, and used to predict magnetic content in water.

Excess quantities of magnetic material in river water can have adverse effects on the health of humans and wildlife [37, 38]. Magnetic material can consist of both heavy metal particulates and dissolved ions with paramagnetic properties. Some notable magnetic contaminants include Cu(II) ions, Iron(III) ions, Chromium(III) ions, particulate aluminum, and particulate manganese. Excess concentrations of these can cause symptoms ranging from neurological problems, organ problems, and cancer [37]. Because of this, being able to study and estimate magnetic material contamination levels quickly with a field deployable system is quite useful. Since NMR is capable of measuring both a reference isotope and paramagnetic material that affects the reference isotope, NMR can be a valuable tool towards studying these contaminants. This section will specifically focus on one of the more common

[1]Daniel Hancock, David P. Wamai, Md Asifuzzaman Khan, Winford Janvrin, Austin R.J. Downey, Mohammed Baalousha, Thomas M. Crawford, Continuous Water Quality Monitoring using Field Deployable NMR and Explainable AI, (2025). Conference proceeding of SPIE Defense + Commercial Sensing. Reprinted here with permission of the publisher, 2025.

paramagnetic contaminants, Cu(II) ions.

The contributions described in this section are twofold: (1) a desktop TD-NMR system has been adapted and temperature controlled for continuous field deployment and; (2) extensive amounts of experimental testing have been done to develop and test a machine learning model to estimate the magnetic content of water. The model implements a random forest trained and tested on data consisting of water quality and NMR measurements from various concentrations of Cu(II) sulfate dissolved in water and is used to estimate Cu(II) ion concentrations in Rocky Branch Creek in downtown Columbia, SC. The data, resultant calculations, data processing techniques, and machine learning methods are hosted in an open-source GitHub repository [17].

3.1 Hardware, Data Collection, and System Validation

This section reports the NMR hardware, in addition to the data collection campaigns and data processing procedures.

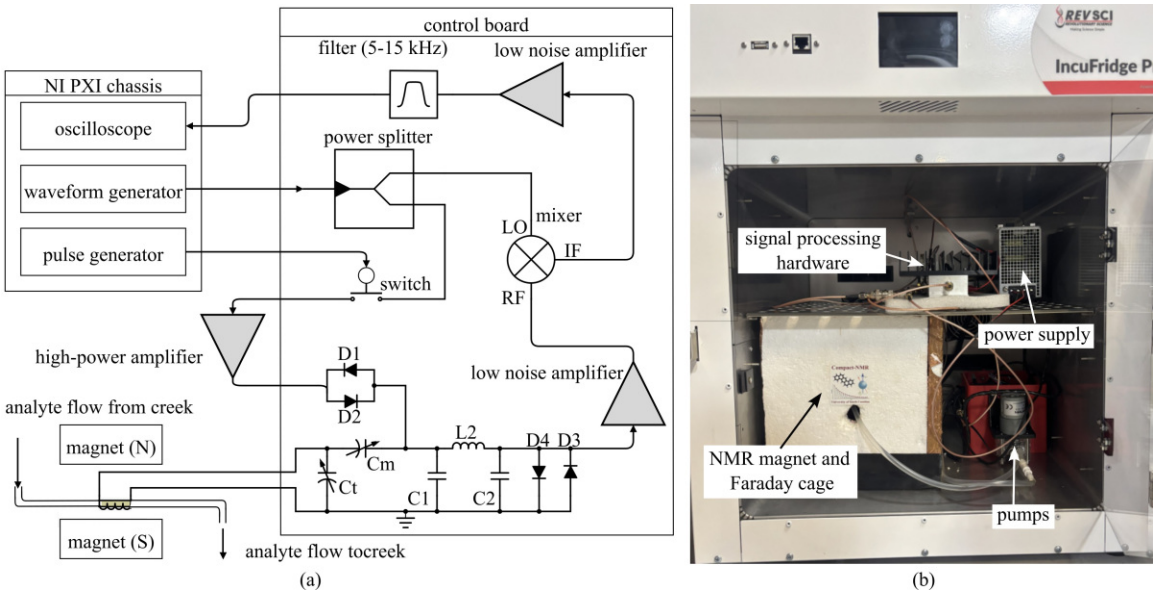

Figure 3.1: Field deployable NMR system setup, showing: (a) the schematic showing the custom electronics for the NMR system (b) the setup inside the environmental chamber.

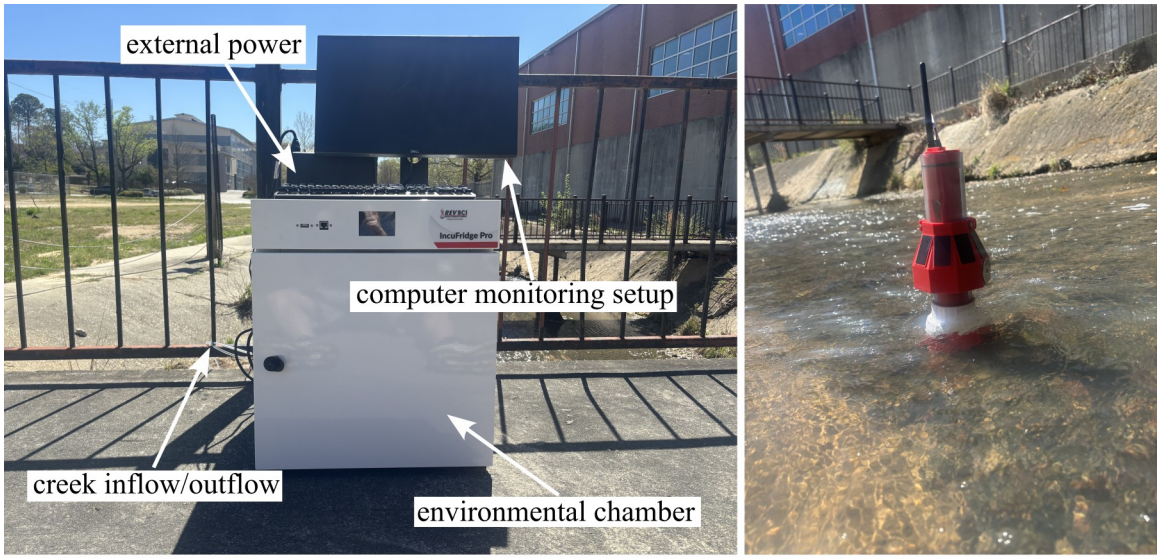

Figure 3.2: System setup showing the: (a) setup deployed at Rocky Branch Creek in Columbia SC, and; (b) the in situ water quality sensor used for measuring the water parameters in situ.

In Situ Nuclear Magnetic Resonance System

This work expands upon the system introduced in Chapter 2 in three primary ways. Firstly, the 0.5 T magnet has been changed to a 0.645 T magnet. Secondly, rather than employing a thunderbolt connection to communicate with an external computer, a NI-PXIe 8821 embedded controller is used to allow the system to function remotely without the presence of an external computer. Lastly, the system was upgraded to be temperature-controlled, applied with Arduino controlled pumps to automatically collect new samples, and equipped with an optional monitor setup to observe measurement progress. The full setup showing the environmental chamber, monitoring equipment, as well as the water quality sensor deployed in the creek, can be seen in Figure 3.2. The system setup used for indoor testing on Cu(II) contaminated water can be seen in Figure 3.1.

While the temperature of the sample itself does not affect the NMR response, there are several other reasons that make this last factor mandatory to consider when

designing a field deployable NMR system. Since a magnet's strength is related to temperature, any changes in temperature directly change the strength of the magnet, affecting the Larmor frequency that can be probed. A change in Larmor frequency doesn't affect the measurements on its own; however, the custom electronics are calibrated to the Larmor frequency at room temperature. If the temperature gets far enough from room temperature, the NMR signal will fade until it is no longer detectable. Even beyond this, changes in temperature cause offsets in the signal passing through operational amplifiers as well as changes in the cutoff frequencies of filters.

Due to the heat generated by the amplifiers and the PXI chassis, heating systems, and air-flow systems do not provide necessary temperature control. To alleviate this, a temperature-controlled environment for the NMR system has been designed utilizing an IncuFridge Pro from Revolutionary Science. Figure 3.1 shows the compact NMR system inside the environmental chamber. On top of the that is equipment for starting data collection. Once data collection has started, the equipment is not needed, however, it can be beneficial to occasionally monitor the collection status. To protect from light weather, the system is placed under a tent, however, it is not recommended to take the system in heavy weather.

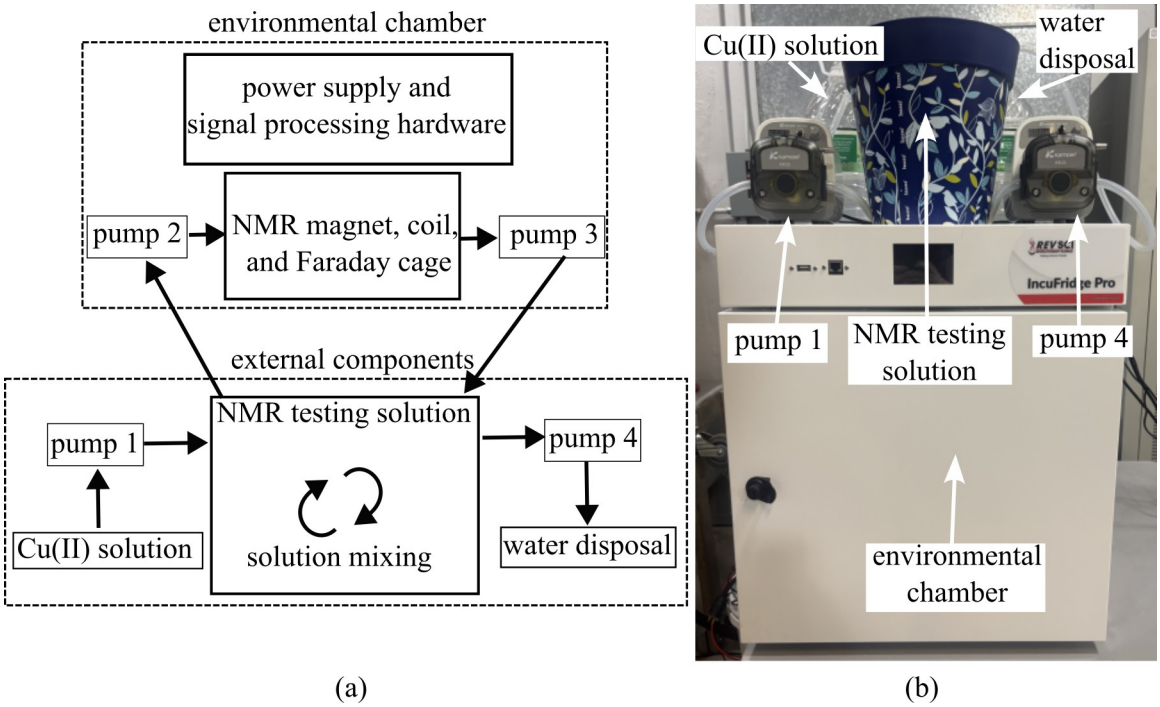

Figure 3.3: System setup showing: (a) diagram of the flow of water through the system (b) laboratory setup used for Cu(II) contaminated water where water contaminated water is pumped through the NMR system.

Data Collection

Data for this work was collected in two ways: continuous measurement from Rocky Branch Creek in Columbia, South Carolina, and continuous measurement on copper-contaminated distilled water in a desktop setup (shown in Figure 3.3). In order to properly train a machine learning model to estimate Cu(II) ion concentrations, it is vital to prepare the training dataset with a wide range of Cu(II) ion concentrations. Determining Cu(II) ion concentration, as well as finding a wide variety of Cu(II) ion concentrations, can be quite a difficult task. Because of this, samples were prepared by using varying concentrations of copper sulfate dissolved in water. Copper sulfate was chosen because while copper is ordinarily diamagnetic, the Cu(II) aqueous ions created when copper sulfate is dissolved in water are paramagnetic, allowing for them to contribute to T2 relaxation. To provide the model with knowledge of a wide range

of contaminant concentrations, solutions ranging from 0 to 1 g/L were created. To give the model additional information regarding lower concentrations, data was taken over the course of several hours while 0.925 L of a 77.3 mg/L solution of Cu(II) ions was slowly and constantly added to 2.86 L of distilled water, while water was being filtered out at the same rate, eventually resulting in a 25mg L solution of copper. Each measurement consisted of NMR data as well as water quality data containing conductivity, temperature, and pH measurements.

Data Processing

The raw NMR data is used to extract a T2 curve from the spin echoes for each measurement by plotting the peak for each spin echo with respect to time. From this T2 curve, an exponential fit is applied according to the following equation

$$M_{xy}(t) = M_0 \exp(-t/T_2), \tag{3.1}$$

where $M_{xy}(t)$ is the magnetization as a function of time, M_0 is the initial magnetization, t is the time, and T2 is the T2 decay constant. From this fit, the T2 time can be calculated.

Table 3.1: T2 curve features used as parameters in the machine learning model.

Feature	Interpretation	Formula
amplitude	initial signal strength	M_0
mean	average value	$\frac{1}{N}\sum_{i=1} N x_i$
standard deviation	distribution around the mean	$\sqrt{\frac{1}{N}\sum_{i=1} N(x_i - \bar{x})^2}$
root mean square	average power	$\sqrt{\frac{1}{N}\sum_{i=1} N x_i^2}$
shape factor	signal shape	$x_{\text{rms}}/\bar{x}$
kurtosis	tail length	$\frac{\frac{1}{N}\sum_{i=1} N(x_i-\bar{x})^4}{[\frac{1}{N}\sum_{i=1} N(x_i-\bar{x})^2]^2}$
skewness	signal asymmetry	$\frac{\frac{1}{N}\sum_{i=1} N(x_i-\bar{x})^3}{\frac{1}{N}\sum_{i=1} N(x_i-\bar{x})^{3/2}}$
impulse factor	ratio of amplitude to mean	$M_0/\bar{x}$
crest factor	ratio of amplitude to RMS	M_0/x_{rms}

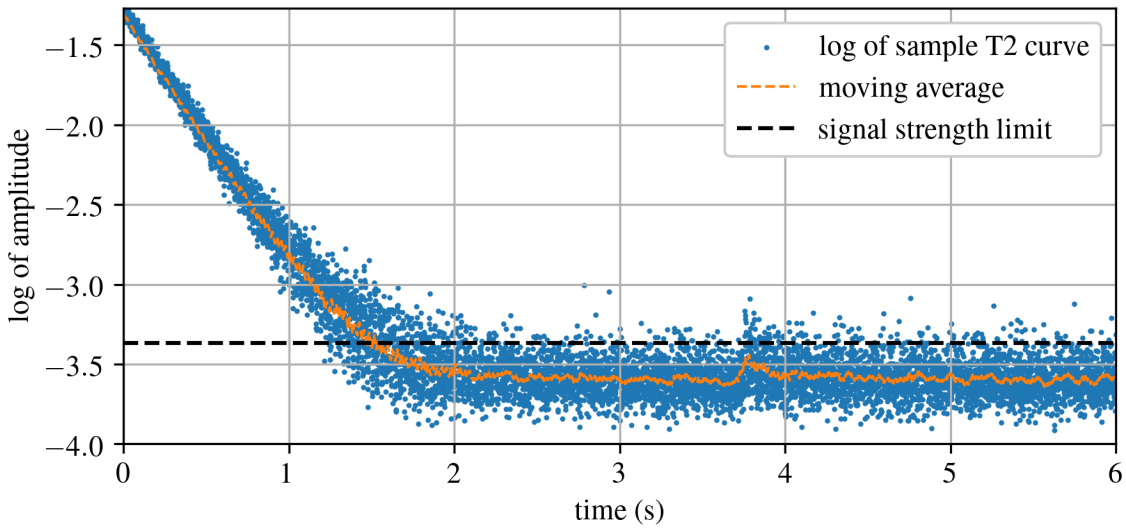

Figure 3.4: Plot showing the log of the T2 data where the horizontal black line is the signal limit of the system.

From the T2 curve, to give the machine learning model more parameters to learn, nine standard time domain features are also calculated. These can be seen in Table 3.1. In total, the collected data and selected features include the T2 time, conductivity, water temperature, pH, amplitude, mean, standard deviation, root mean square, shape factor, kurtosis, skewness, impulse factor, and crest factor, resulting in 13 total parameters. Each of these parameters, as well as the T2 time were calculated after truncating the data in each measurement as its NMR signal decayed to the noise level of the system. This was done by calculating a signal limit for each measurement by looking at the logarithm of the measurement and averaging the mean and the maximum of the remaining noise after the signal finished decaying. A visual representation of this can be seen in Figure 3.4.

3.2 Machine Learning Implementation

The explainable machine learning approach utilizes a random forest which was chosen due to its ease of implementation, need for little data preprocessing, robustness to overfitting, and interpretability [27]. To train the model, the dataset consisting

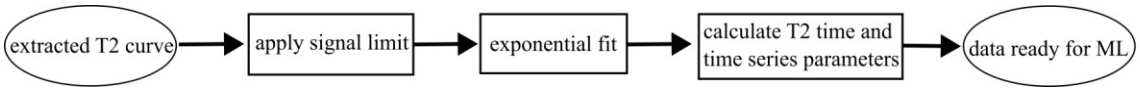

Figure 3.5: Flowchart showing the data processing and machine learning model training tasks.

of measurements from distilled water and Cu(II) contaminated distilled water was randomly split into 70 percent training and 30 percent testing datasets. The model was trained with a 10-fold cross-validation while hyperparameters, specifically the maximum tree depth, the number of trees, the minimum samples per leaf, and the minimum samples needed to split the tree, were auto-tuned using a grid search. The best-performing random forest, determined by mean square error on the test dataset was returned and re-trained on the full test dataset. This resultant model was then used to estimate the magnetic content of the water from the dataset collected from Rocky Branch Creek. A flowchart showing the data processing and machine learning steps can be seen in Figure 3.5. Algorithm 1 describes the process of taking data from the Cu(II) contaminated measurements to train the model and inputting data from Rocky Branch Creek measurements into the model to provide an estimation of Cu(II) ion concentration.

To further understand the model, the feature importance and the partial dependence of the features were calculated on both the test dataset and the estimated dataset. Feature importance can be used to show how important each feature is when the model is making decisions. Partial dependence plots can be used to show how each feature affects the estimated parameter of the model. For example, a horizontal line shows that the feature has little effect on the model's estimation while a sloped line shows that as the feature increases/decreases, the estimated parameter increases/decreases as well. While similar, feature importance and partial dependence are calculated differently so including both helps to ensure the model's estimations are made in a reasonable way.

Algorithm 1 Pseudocode describing how estimations of Cu(II) ion concentration are created.

```
BEGIN
INPUT data = [T2, water_quality, time_series_features]
INPUT mp_concentration
params = (data, mp_concentration)
model = model_cross_validate(params)
model = model_hyperparameter_search(model)
model = get_best_model(model)
model.train(params)
INPUT creek_data = [T2_creek, water_quality_creek, time_series_features_creek]
mp_estimations = model.predict(creek_data)
OUTPUT mp_estimations // units of mg/L
END
```

3.3 Results

Figure 3.6 shows the T2 data and conductivity measurements throughout data collection for the Cu(II) contaminated dataset. Since this data was collected over the course of several weeks with breaks between collections, black dotted lines are used to denote these breaks. As expected, there is a clear relationship between T2 time and conductivity, although that relationship gets decreasingly clear as Cu(II) ion concentration approaches zero. Figure 3.7 shows how all other measured and calculated features changed throughout the measurement

The machine learning model estimated the Cu(II) ion concentration on the test dataset with a mean squared error of 12.2 mg^2/L^2 and an R^2 of 0.998. Figure 3.8 shows a scatterplot comparing the estimated Cu(II) ion concentrations to the actual Cu(II) ion concentrations. Figure 3.9 shows a partial dependence plot, indicating that low T2 times and low conductivity measurements are used by the model to estimate high magnetic content while with high T2 times, the model uses high conductivity measurements along with very slight input from water temperature and pH.

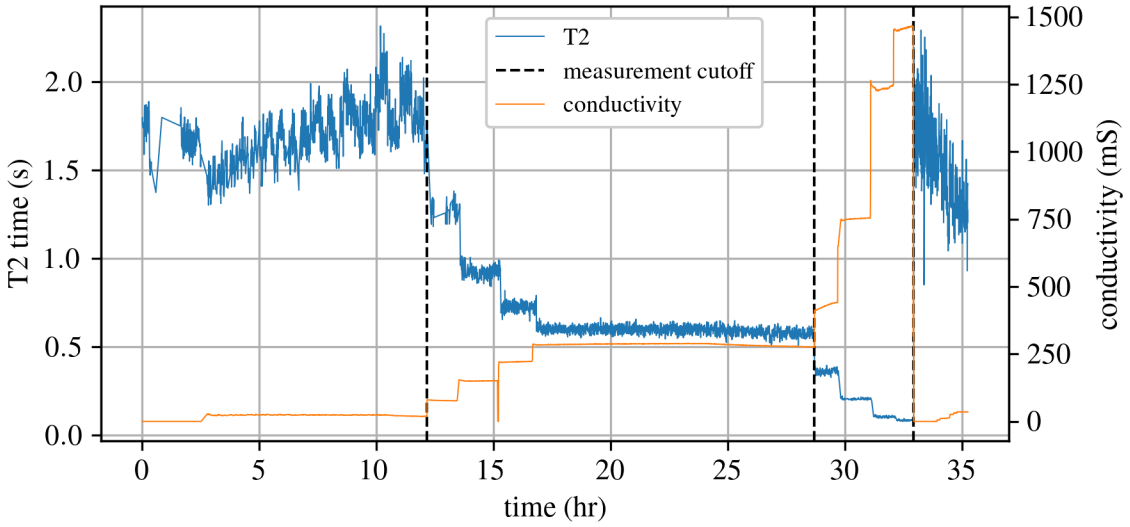

Figure 3.6: Cu(II) contaminated data showing T2 data and conductivity data over time. The vertical black dotted lines show where data collection was halted and started again at a later date.

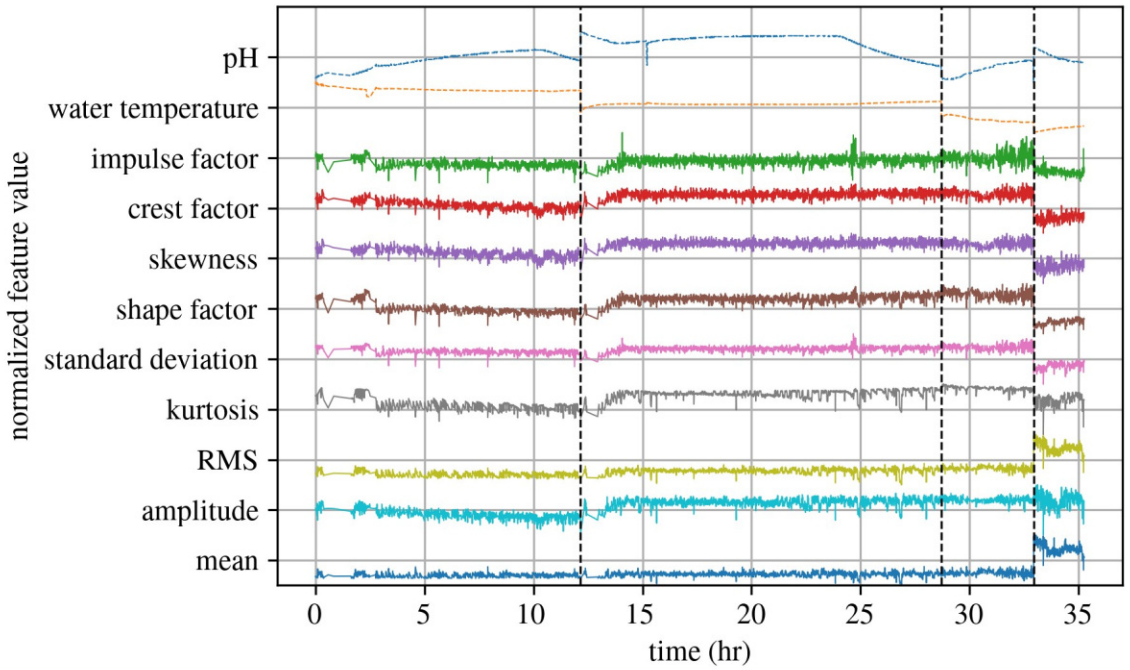

Figure 3.7: Cu(II) contaminated data showing all other measured parameters over time, with solid lines representing time series data and dotted lines representing water quality data. The vertical black dotted lines represent where data collection was halted and resumed at a later date.

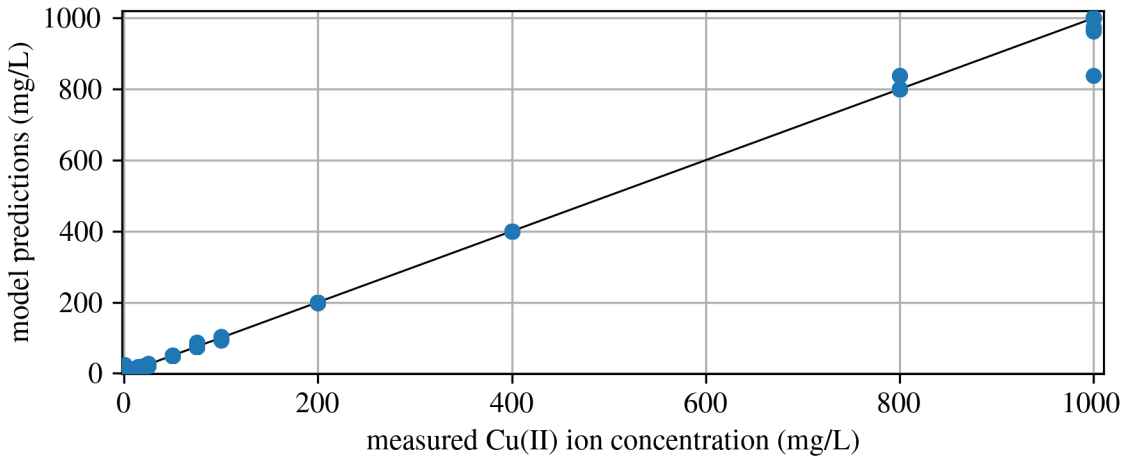

Figure 3.8: Cu(II) contaminated data showing a comparison between the values of Cu(II) ion concentration estimated by the model with the actual measured values.

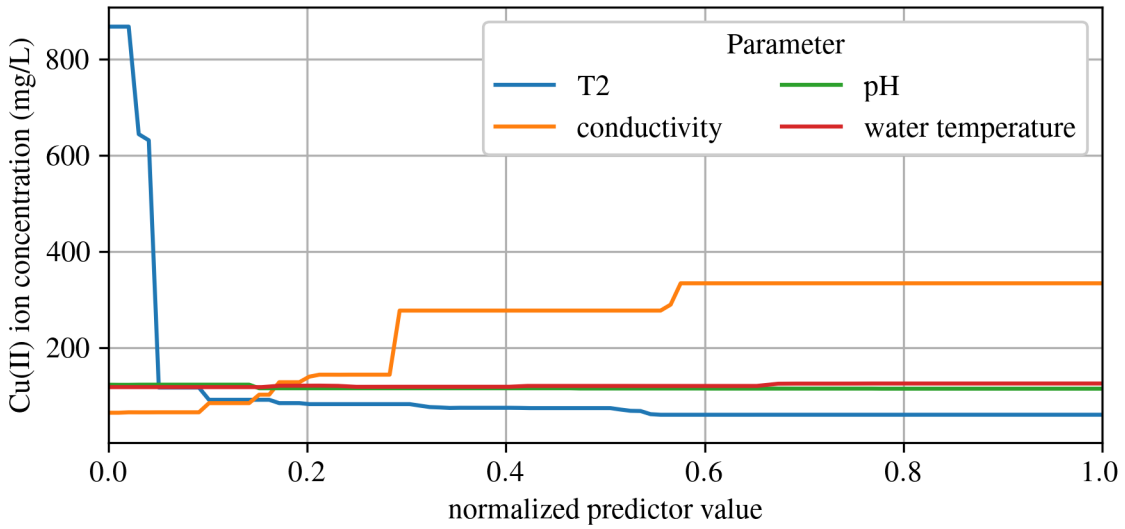

Figure 3.9: Partial dependence plot for the Cu(II)-contaminated laboratory dataset, illustrating how each data-driven feature influences the model's estimations.

A feature importance chart is shown in Figure 3.10, where the bars show the importance and the black lines show the standard deviation, indicating that T2 and conductivity are by far the most important features regarding the model's decision-making, followed distantly by pH and water temperature. Feature importance and partial dependence both agree that the T2 time and the conductivity measurements

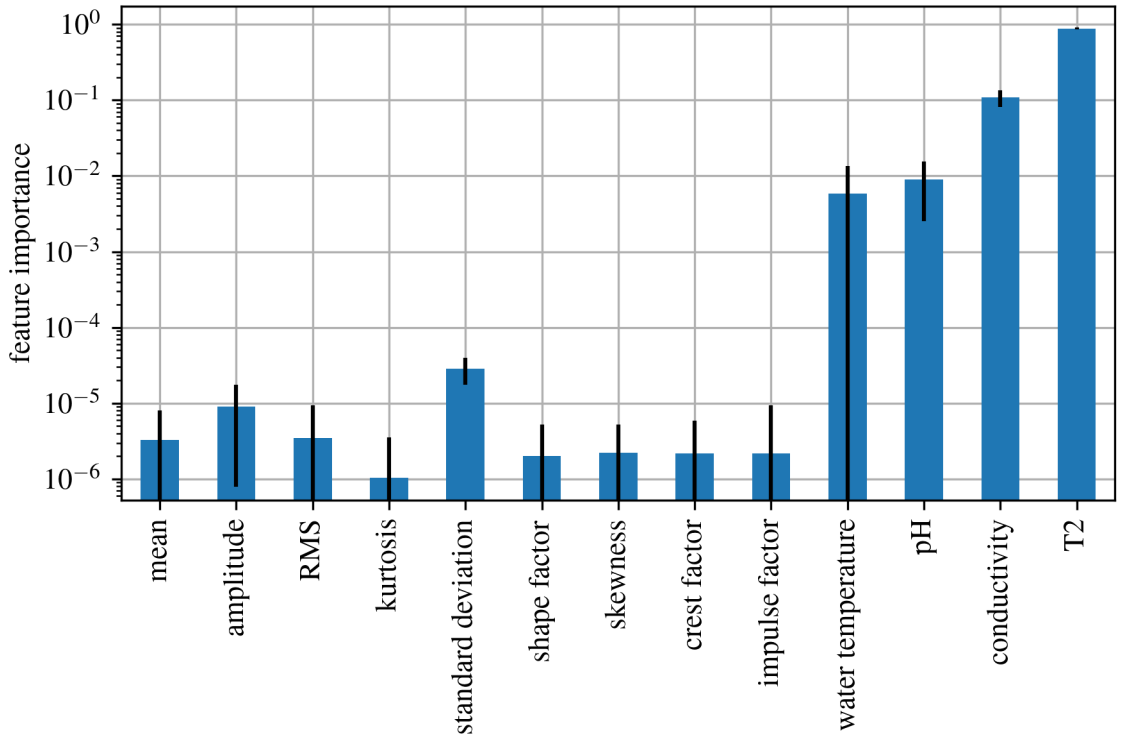

Figure 3.10: Trained on Cu(II) contaminated data, this is a plot indicating how important each feature is to the decisions made by the model.

are most influential to the model, showing that the model not only makes correct estimations, but that it does so with correct reasoning.

Figure 3.11 shows the T2 times as well as the conductivity measurements over time at Rocky Branch Creek. T2 stays fairly consistent throughout the measurement, with only comparatively small deviations. The conductivity data shows consistent changes with a peak near the 10-hour mark, although relatively small in magnitude. While conductivity should be an indicator of Cu(II) ion concentration, it should be noted that not all dissolved solids are magnetic. So while a relationship between conductivity and T2 time is expected, not all changes in conductivity will cause a change in T2 time. Additionally, the standard deviation of the conductivity sensor is used to show that while the conductivity data drifts, it remains statistically similar throughout the measurement. This standard deviation was calculated on a dataset consisting of 1500 data points at a known, constant concentration of conductivity.

Figure 3.12 shows how all of the other measured and calculated features change throughout the measurement. Several of the features such as RMS and standard deviation are much noisier in this data compared to the Cu(II) contaminated data. This is to be expected since T2 measurements are much noisier in this dataset.

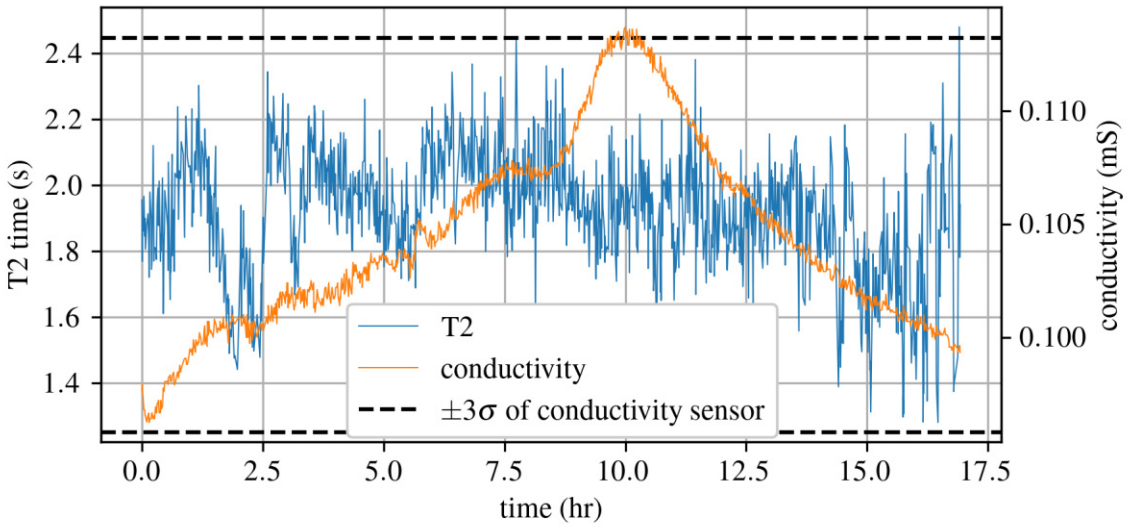

Figure 3.11: Data collected from Rocky Branch Creek showing T2 measurements time and conductivity measurements over time, as well as the standard deviation of the conductivity sensor.

The estimated Cu(II) ion concentrations from the dataset using water from Rocky Branch Creek are shown in Figure 3.13. Throughout the entire measurement, the Cu(II) ion concentrations are estimated to be on the low end of the system's resolution, between 6.5 and 12.5 mg/L. From 0 to 1 hr, there is a sharp increase in the estimated Cu(II) ion concentration. While it is unclear exactly what caused this increase, that portion of the dataset does have the lowest conductivity and the highest pH measurements of the dataset, likely influencing the model's behavior in that section. After approximately the 1-hour mark, the estimated Cu(II) ion concentration is fairly constant. A partial dependence plot for the model's estimations on data from Rocky Branch Creek can be seen in Figure 3.14 showing that the most important features of the model influence the consistency of the estimations.

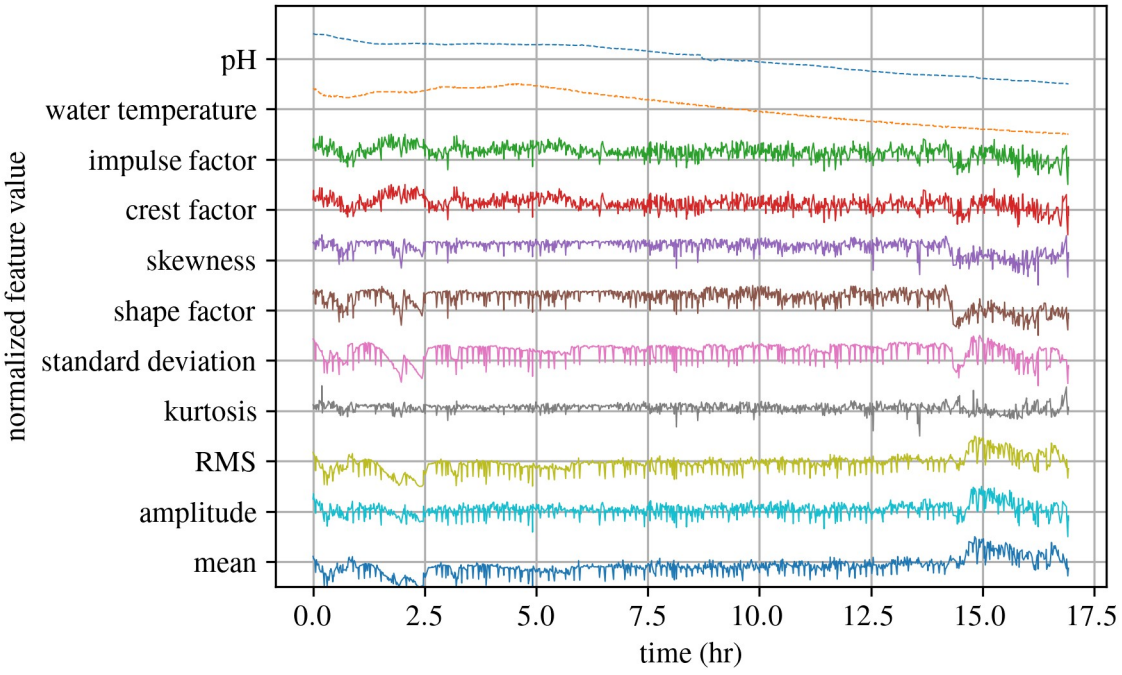

Figure 3.12: Rocky Branch Creek data showing all other measured parameters over time, with solid lines representing time series data and dotted lines representing water quality data.

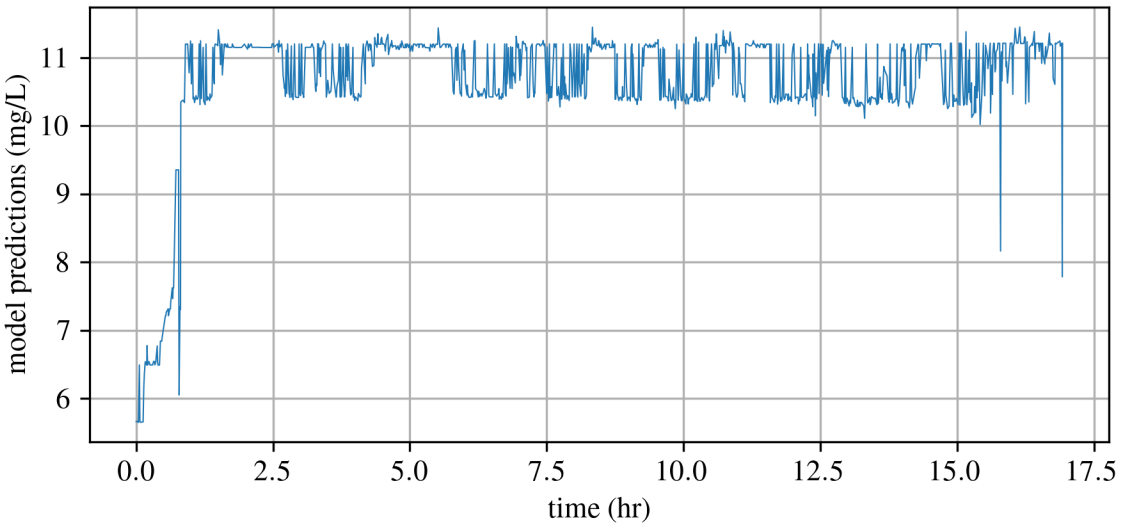

Figure 3.13: Rocky Branch Creek estimations showing the model's calculations for Cu(II) ion concentration.

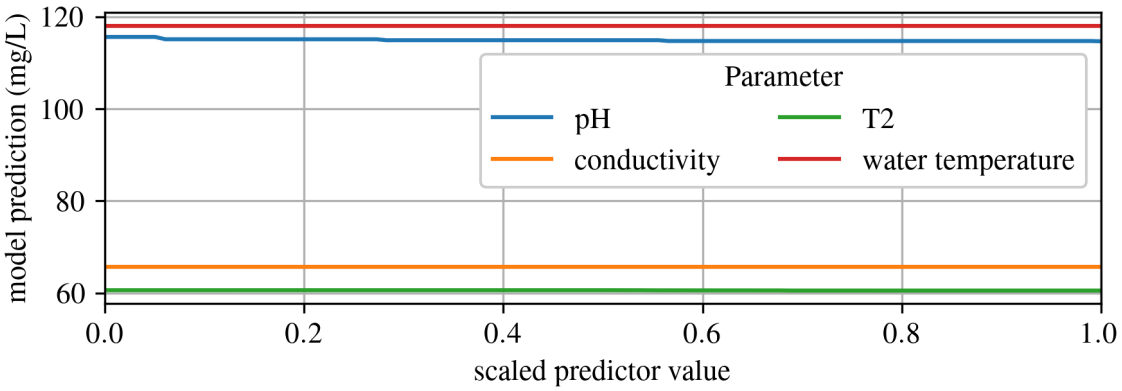

Figure 3.14: Rocky Branch Creek data showing the partial dependence plot indicating how each of the model features affects the decision-making of the model.

3.4 Conclusion

This chapter presents a TD-NMR system that is capable of being deployed for continuous monitoring of Cu(II) ion concentration in water systems. The NMR system is temperature-controlled and remotely operated with an embedded system, allowing for continuous, high-quality relaxation data to be collected. The extensive dataset generated in this work to train the random forest model consists of NMR and water quality data on wide ranges of Cu(II) ion concentrations. The model was trained on the dataset utilizing a ten-fold cross-validation as well as the autotuning of hyperparameters via a grid search, resulting in a mean squared error of 12.2 mg^2/L^2 and an R^2 of 0.998. In line with expectations, the most important features used by the model are the T2 time and the conductivity measurements. This model was used to estimate the Cu(II) ion concentration of data acquired from Rocky Branch Creek. The results showed fairly constant estimations at the low end of the system's resolution, in line with the consistency of the T2 time and conductivity measurements. The sharp increase at the beginning of the estimations may be related to the local minima and maxima of conductivity and pH respectively, although it is unclear. The overall magnitude of the predictions were high than the amount of Cu(II) expected to be in Rocky Branch Creek, suggesting that there was likely other magnetic ma-

terial in the water. Future work will be done to investigate the possibility of using Cu(II) concentration to be able to predict total magnetic contamination, perhaps by looking at contaminant dipole moment per volume. Overall, the system and model implemented in this chapter host the capability of providing real-time estimations of Cu(II) ion concentration while being deployed remotely near waterways.

Acknowledgments

This material was sponsored by the National Science Foundation, United States under Grant Nos. CMMI-2152896, CPS-2237696 and ITE-2344357. The views and conclusions contained within this document are those of the authors and should not be interpreted as representing the official policies of the NSF or the U.S. Government.

Chapter 4

Conclusion

Leveraging the powerful technique of spin-spin relaxation, an open-source TD-NMR system has been created with capabilities of use for a variety of purposes such as fat, hydrocarbon fuel, and magnetic particle characterization. The system was tested for validity, verifying a linear relationship between Cu(II) ion concentration and T_2 rate. With this, the system was adapted to be used for field deployment, made possible by the implementation of temperature control, the addition of a flow-through system via Arduino controlled pumps, and the transition from thunderbolt connection with external computers to an embedded controller that enables remote data collection. Additionally, a machine learning framework to use with T2 data has been developed. To do this, data containing measured concentrations of Copper (II) sulfate were collected and used as training and testing data for a machine learning model utilizing random forests. The trained model was able to accurately describe this data, resulting in a mean squared error of 50.21 mg^2/L^2 and an R^2 coefficient of 0.998. Data was then collected at Rocky Branch Creek with unknown Cu(II) concentrations to be predicted by the machine learning model. While the predictions have yet to be verified experimentally, the predicted ranges lie within expectation, showcasing the promising ability of this system and model to be able to remotely measure Cu(II) concentration in seconds.

There are many ways this system and model can be improved upon in the future. Taking data during field deployment while measuring Cu(II) concentration via alternative methods will provide the model with quantitative analysis of its predictions on

data that is not currently in the training dataset. Additionally, to aid the model in learning relationships between all of the features at concentrations of Cu(II) where T_2 alone would not provide definitive results, a much expanded training dataset focusing on Cu(II) concentrations below 15 mg/mL would be helpful. It should also be investigated whether or not it is possible to use Cu(II) contaminated data to generalize for magnetic contaminants in general. While there is a linear relationship between magnetic contamination and T2 rate, the slope differs for different contaminants due to differences of the magnetic moment of the contaminant. It may be possible to generalize the contamination to magnetic moment per volume added to a distilled water solution to expand the effectiveness of the model. To help deploy the system to rivers more easily, a smaller temperature controlled box, rather than a fridge would be beneficial. Furthermore, working with (^{1}H) NMR, it is only possible to detect molecules containing Hydrogen as well as magnetic substances that affect the Hydrogen nuclei. To alleviate this, ligands are often used in NMR. These ligands are Hydrogen-containing molecules that can temporarily attach with ions in the water so that a (^{1}H) NMR signal can be found. Injecting and then removing ligands in the flow-through system would greatly increase the amount of detectable contaminants in water.

Looking at broader long-term goals, in the future, this system may be used to not only measure quantities of certain contaminants, but to distinguish between different contaminants based on the T2 data. To do this, there are two main things to consider: multi-exponential fitting rather than single exponential fitting and taking the Fourier transform of the time series to check for peaks characteristic of multiple contaminants. While it is possible the resolution of this system is not high enough to resolve peaks aside from the main component of the sample, it is important to investigate the possibility of this technique.

Overall, the system described in this thesis serves as a strong foundation for

a growing NMR program seeking to deliver remote, field deployed NMR systems capable of measuring and distinguishing contaminants within seconds.

Appendix A

Permission to Reprint

A.1 CHAPTER 2: HardwareX

Dear Prof. Daniel Hancock,

Thank you for contacting us.

As an Elsevier journal author, you retain the right to Include the article in a thesis or dissertation (provided that this is not to be published commercially) whether in full or in part, subject to proper acknowledgment; see https://www.elsevier.com/about/policies/copyright for more information. As this is a retained right, no written permission from Elsevier is necessary.

As outlined in our permissions licenses, this extends to the posting to your university's digital repository of the thesis provided that if you include the published journal article (PJA) version, it is embedded in your thesis only and not separately downloadable.

Thank you.

Kind regards,

Thomas Rexson Yesudoss
Copyrights Specialist
ELSEVIER | HCM - Health Content Management

Visit Elsevier Permissions

A.2 CHAPTER 3: The International Society for Optics and Photonics, Smart Structures + Nondistructive Evaluation

Hello and good day,

SPIE grants to authors (and their employers) of papers, posters, and presentation recordings published in SPIE Proceedings or SPIE Journals on the SPIE Digital Library (hereinafter "publications") the right to post an author-prepared version or an official version (preferred) of the publication on an internal or external server controlled exclusively by the author/employer or the entity funding the research, provided that (a) such posting is noncommercial in nature and the publication is made available to users without charge; (b) an appropriate copyright notice and citation appear with the publication; and (c) a link to SPIE's official online version of the publication is provided using the item's DOI.

This authorization extends to noncommercial third-party platforms such as Zenodo in instances where the author's institution uses those platforms as their institutional repository.

This authorization does not extend to third-party web sites not owned and maintained by the author/employer such as ResearchGate, Academia.edu, YouTube, etc.

Lisa M. Haley
Proceedings Coordinator
SPIE – the international society for optics and photonics
lisah@spie.org

Tel: +1 360 685 5603
Fax: +1 360 647 1446

SPIE.

Bibliography

[1] Ismaila Abdullahi, *Magnetic resonance imaging of copper corrosion*, Ph.D. thesis, University of Birmingham, 2014.

[2] Belal M.K. Alnajjar, André Buchau, Lars Baumgärtner, and Jens Anders, *NMR magnets for portable applications using 3D printed materials*, **326**, 106934.

[3] Yoshimi Anzai and Linda Moy, *Point-of-care low-field-strength MRI is moving beyond the hype*, **305**, no. 3, 672–673.

[4] ARTS-Lab, *Compact-NMR*, GitHub.

[5] Bernhard Blümich, *Introduction to compact NMR: A review of methods*, **83**, 2–11.

[6] Bernhard Blümich and Kawarpal Singh, *Desktop NMR and its applications from materials science to organic chemistry*, **57**, no. 24, 6996–7010.

[7] Bernhard Blümich, Christian Rehorn, and Wasif Zia, *Magnets for small-scale and portable NMR*, pp. 1–20.

[8] Peter Blümler and Helmut Soltner, *Practical concepts for design, construction and application of Halbach magnets in magnetic resonance*, **54**, no. 11–12, 1701–1739.

[9] Nicholas Bryden, Michael Antonacci, Michele Kelley, and Rosa T. Branca, *An open-source, low-cost NMR spectrometer operating in the mT field regime*, **332**, 107076.

[10] H. Y. Carr and E. M. Purcell, *Effects of diffusion on free precession in nuclear magnetic resonance experiments*, Phys. Rev. **94** (1954), 630–638.

[11] LibreTexts Chemistry, *Supplemental modules (physical and theoretical chemistry*, 2023.

[12] Allen D. Elster, *Dipole-dipole interactions*, 2024.

[13] ———, *Paramagnetic relaxation*, 2024.

[14] ———, *Spin-spin relaxations*, 2024.

[15] ———, *T2 relaxation: Definition*, 2024.

[16] Melvina C. Ezeanaka, John Nsor-Atindana, and Min Zhang, *Online low-field nuclear magnetic resonance (LF-NMR) and magnetic resonance imaging (MRI) for food quality optimization in food processing*, **12**, no. 9, 1435–1451.

[17] Daniel Hancock, David P. Wamai, Md Asifuzzaman Khan, Austin R.J. Downey, Mohammed Baalousha, and Thomas M. Crawford, *Paper-2025-continuous-water-quality-monitoring-using-field-deployable-NMR*, GitHub, 2025.

[18] Lars G. Hanson, *Is quantum mechanics necessary for understanding magnetic resonance?*, Concepts in Magnetic Resonance Part A **32A** (2008), no. 5, 329–340.

[19] Joseph P. Hornak, *The basics of NMR*, 2019.

[20] Parker Huggins, Win Janvrin, Jake Martin, Ashley Womer, Austin R. J. Downey, John Ferry, Mohammed Baalousha, and Jin Yan, *Assessing magnetic particle content in algae using compact time domain nuclear magnetic resonance*, Ocean Sensing and Monitoring XVI (Weilin Hou and Linda J. Mullen, eds.), vol. 6, SPIE, p. 1.

[21] Parker Huggins, Jacob S. Martin, Austin R.J. Downey, and Sang Hee Won, *Interpretable machine learning for predicting the derived cetane number of jet fuels using compact TD-NMR*, 137018.

[22] S Iguchi, R Piao, M Hamada, S Matsumoto, H Suematsu, T Takao, A T Saito, J Li, H Nakagome, X Jin, M Takahashi, H Maeda, and Y Yanagisawa, *Advanced field shimming technology to reduce the influence of a screening current in a REBCO coil for a high-resolution NMR magnet*, Superconductor Science and Technology **29** (2016), no. 4, 045013.

[23] National Instruments, *PXI-5124 specifications*, February 2023.

[24] Winford Janvrin, Jacob Martin, Daniel Hancock, Austin Downey, Perry Pellechia, Joud Satme, and Sang Hee Won, *Open-source compact time-domain hydrogen (1H) nmr system for field deployment*, (2025).

[25] Simon Kern, Klas Meyer, Svetlana Guhl, Patrick Graber, Andrea Paul, Rudibert King, and Michael Maiwald, *Online low-field NMR spectroscopy for process control of an industrial lithiation reaction-automated data analysis*, **410**, no. 14, 3349–3360.

[26] Alain Louis-Joseph and Philippe Lesot, *Designing and building a low-cost portable FT-NMR spectrometer in 2019: A modern challenge*, **22**, no. 9-10, 695–711.

[27] Scott M. Lundberg, Gabriel Erion, Hugh Chen, Alex DeGrave, Jordan M. Prutkin, Bala Nair, Ronit Katz, Jonathan Himmelfarb, Nisha Bansal, and Su-In Lee, *From local explanations to global understanding with explainable AI for trees*, **2**, no. 1, 56–67.

[28] Roger S. Macomber, *A complete introduction to modern NMR spectroscopy*, Wiley, New York, 1998.

[29] Jacob Martin, Austin R.J. Downey, and Sang Hee Won, *Compact time domain NMR design for the determination of hydrogen content in gas turbine fuels*, Volume 1: 24th International Conference on Advanced Vehicle Technologies (AVT), American Society of Mechanical Engineers, aug 2022.

[30] Jacob S. Martin, Austin R. J. Downey, Mohammed Baalousha, and Sang Hee Won, *Rapid measurement of magnetic particle concentrations in wildland-urban interface fire ashes and runoff using compact NMR*, **24**, no. 6, 7355–7363.

[31] David C. Meeker and M Priboianu, *Finite element method magnetics*, 2002.

[32] Giorgio Moresi and Richard Magin, *Miniature permanent magnet for table-top NMR*, Concepts in Magnetic Resonance Part B: Magnetic Resonance Engineering **19B** (2003), no. 1, 35–43.

[33] Sarah Mandy Nagel, Christoph Strangfeld, and Sabine Kruschwitz, *Application of 1h proton NMR relaxometry to building materials - a review*, **6-7**, 100012.

[34] The Electronic Code of Federal Regulations, *Part 18—industrial, scientific, and medical equipment*, February 2025.

[35] Dmytro Polishchuk and Han Gardeniers, *A compact permanent magnet for microflow NMR relaxometry*, **347**, 107364.

[36] H. Raich and P. Blümler, *Design and construction of a dipolar Halbach array with a homogeneous field from identical bar magnets: NMR mandhalas*, **23B**, no. 1, 16–25.

[37] Veer Singh, Nidhi Singh, Sachchida Nand Rai, Ashish Kumar, Anurag Kumar Singh, Mohan P. Singh, Ansuman Sahoo, Shashank Shekhar, Emanuel Vamanu, and Vishal Mishra, *Heavy metal contamination in the aquatic ecosystem: Toxicity and its remediation using eco-friendly approaches*, Toxics **11** (2023), no. 2, 147.

[38] Sudarningsih Sudarningsih, Aditya Pratama, Satria Bijaksana, Fahruddin Fahruddin, Andi Zanuddin, Abdus Salim, Habib Abdillah, Muhammad Rusnadi, and Mariyanto Mariyanto, *Magnetic susceptibility and heavy metal contents in sediments of Riam Kiwa, Riam Kanan and Martapura rivers, Kalimantan Selatan province, Indonesia*, Heliyon **9** (2023), no. 6, e16425.

[39] Michael C.D. Tayler and Sven Bodenstedt, *NMRduino: A modular, open-source, low-field magnetic resonance platform*, **362**, 107665.

[40] Lizhi Xiao, Guangzhi Liao, Feng Deng, Huabing Liu, Gongpu Song, and Mengchun Li, *Development of an NMR system for down-hole porous rocks*, **205**, 16–20.